Politecnico di Torino

Investigation of mass transport in porous media for desalination purposes

Master degree in mechanical engineering

Candidate: WANG ZEYU
Supervisor: CHIAVAZZO ELIODORO (DENERG)
Co-supervisor: MORCIANO MATTEO (Docente esterno)

Collegio di Ingegneria Meccanica, Aerospaziale, dell'Autoveicolo e della Produzione

Date of defense: 14/10/2021

Contents

Abstract

Shortage of fresh water resources is a major problem that human has been faced, especially in some remote mountains and islands where were lack of electricity. Solar desalination technology is an effective method to satisfy the need for drinkable water resources in some regions which are far away from cities or short of power, like islands and villages near the sea. In order to have a progress in developing this technology there are some critical issues should be focused on, like the materials should be inexpensive, the technology should be easy-to-applied, and devices should be able to run without too much maintenance and keep the stable supply of fresh water for local resident. Nevertheless, there's a big barrier in front of us, how to avoid the accumulation of salt on the device so that the fresh water production rate is not affected by it during the working process. In this passage, a type of solar passive distiller with several stages is discussed. This technology helps solving the challenge mentioned before very well (stable and better performance with salt rejection at the same time) by optimizing the configuration. Here to make it clear why the salt accumulation is not happened in this device, which means the mass transport here is more effective than the pure diffusion phenomenon, an integrated theory is given. In this paper, the Marangoni effect at the water-air interface is considered for the reason of the concentration differences and thus the surface tension. The simulation results showed that the salt rejection ability of this device is good enough to cope with the clogging during the whole desalination process. In addition, the same device with different configurations will have different salt rejection performances. Thus, this study can be an inspiration on how to optimize the performance of the solar passive desalination device by changing the structure so that this technology can be broadly adopted in rural areas with hard access with fresh water resources in a dependable way.

1. Introduction

1.1. About desalination

As the source of all life on the earth, water is also one of the indispensable basic substances for human survival and industrial production, an irreplaceable precious natural resource, and one of the controlling elements of the ecological environment on the earth. Although two-thirds of the earth's surface is covered by water, seawater that cannot be directly drunk or used for irrigation due to its high salinity accounts for 97% of the total water on the earth, and only 1% is freshwater resources, in addition, the distribution of freshwater resources is extremely uneven. With the rapid growth of population and the continuous development of industry and agriculture, on the one hand, the demand for fresh water will increase rapidly. On the other hand, due to the large amount of waste discharged by industry, a large number of clean water resources such as rivers and lakes are affected and this also caused severe pollution and destruction of scarce freshwater resources. In the future, many countries will face the problem of shortage of freshwater resources[1-4]. Since the seawater is the most abundant water resource, and it is of great significance to solve the current shortage of freshwater resources through desalination. Therefore, in coastal areas and islands with abundant seawater resources, giving full play to the seaside advantages and using desalination technology is a practical and sustainable way to solve the problem of water shortage in these areas. For this reason, after entering the new century, it is considered by all countries in the world to be the most feasible and economical way to obtain fresh water.[5]

As we all know, the desalination process is to separate fresh water from the salt water. So, it's very important to find a way to do this. There are already kinds of ways, the key theory behind these all methods is to separate the solid salt from the liquid water by making use the specific energy. From history record, the earliest desalination devices for drinkable water were inspired by the evaporation process (when the water is heated up to a temperature there will be vapor and that can be fresh water when being condensed). And the energy of heat can from the sun or burning of some material (wood or coal etc.). Although this process is energy wasting in most cases (except solar energy), it is still adopted to get fresh water as the principle of many desalination technologies.

With the rapid development in material science in recent decades, a new type of material-semi-permeable membranes is found to be very suitable for the desalination process. The reason is that only some specific size or type of ions are able to enter or exit the membrane, thus separating the salt from the water.

1.2. State of art of solar desalination technology

All in all, in accordance with the type of energy employed in desalination process, all

kind of technologies can be divided like this (see Fig. 1.1)[6]

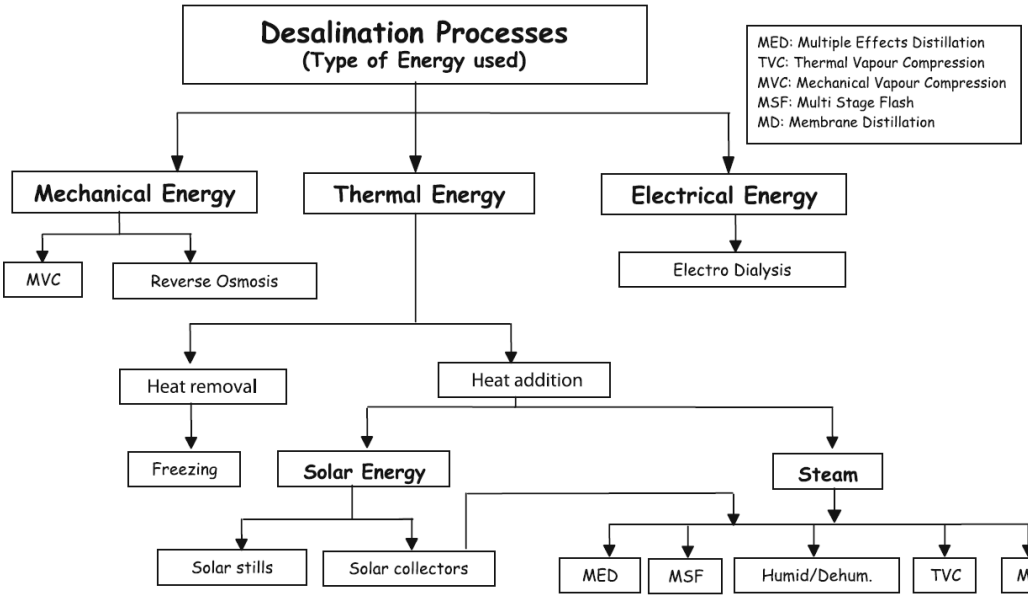

Fig. 1.1 Desalination technologies classification according to the type of energy used [6](Picture taken from Ref.[6], with permissions)

Among these technologies, solar desalination technology is the simplest technology which adopts solar energy as an inexhaustible and renewable energy source for distillation of the sea water[7] [8].

Here some efficient, stable, easy to maintain and relatively simple desalination devices able to be applied in emergency conditions have been recently designed and studied in literature[9-19].

In 2009, A.E. Kabeel and co-workers proposed an experimental investigation on a new design of solar still with wicked concave surface [9].

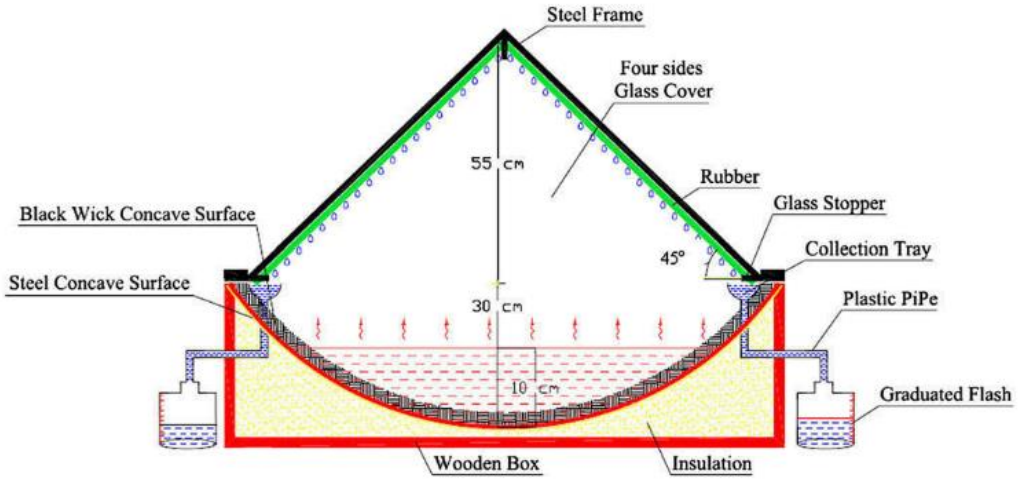

Fig. 1.2 Schematic diagram of concave-based passive distiller.[9](Picture taken from Ref.[9], with permissions)

In order to get the experimental data, a concave-shaped solar passive distiller with wick is designed and fabricated. Here in Fig. 1.2 and Fig. 1.3 the schematic diagram and the real model of this device are demonstrated respectively. This device is mainly composed of seven parts, namely steel frame, glass cover, rubber, collection system,

wooden box, insulation and wick. On the top side, there are four glass covers placed at 45 degrees with respect to horizontal and whose thickness is 3mm so that the sunlight can reach the wick, and one of them should be orientated towards south during the experimental. Beneath the glass cover there is a layer of silicone rubber which can be the seal and prevent the vapor from escaping from the device thus causing losing of energy. On both left and right sides there is a collection system which constitutes of steel-made funnel, plastic pipes and bottles which is used to collect the final fresh water. Then the main container at the bottom is mainly composed of four parts. The outside box is made from wood whose thickness is 5cm for supporting the whole device and also thermal insulation. The insulation layer is also for the same reason. The steel concave surface is in square shape whose size is $1.2\ m \times 1.2\ m$ with a thickness of 2mm. On the top of that there is a wick surface with the same size, a part from that, in order to maximize the absorbed solar energy, the black wick is chosen. The height from the most bottom part of the basin to the highest place is 30cm, and it can contain 10cm height of water during the experimental. In order to calculate the efficiency of this device, there are some important data should be recorded during the process. For example, some temperatures on different parts of the device (the wick, the glass and the container), Also, the intensity of solar radiation should be monitored at all times during all the tests.

Fig. 1.3 A demonstration of the concave-based passive distiller.[9] (Picture taken from Ref.[9], with permissions)

According to the data recorded from the tests and all the results during the whole day, their concave-based passive distiller can reach the productivity of 4.0 l/m^2 and the efficiency is about 45%. In conclusion, this device reaches a good performance by utilizing larger area for absorbing the solar energy and also the wick to improve the evaporation process. However, the basin needs to be added with salt water regularly and also the clogging of the wick will be a problem to keep the stable fresh water production.

Afterwards, Zerrouki, Moussa and his co-workers proposed a capillary film solar still coupled with a conventional solar still[10]. In this work, the main objective is to discuss three passive distillers with different configurations. The first device is based on the capillary forces, the second one is the first generation of the distiller and the last one is the most complex one among them, and this device can be seen as a combination of the first one (with capillary film) and the second one (see Fig. 1.4, Picture taken from Ref.[10], with permissions). Here the device can be seen as a two-stage distiller, in each stage there is a glass cover, and fresh water collection system, but in first stage there is the wick. The overall process can be described as this: the salt water in the tank with a concentration of 1-3g/l is risen up on the wick for the reason of capillary forces. In first step, this water is evaporated by the solar energy through the first glass cover during it flowing in the wick, then some of the water will be condensed by the condenser plate and then will be collected by the funnel. The rest of the water with a relatively high salt concentration of around 1.84-5.5g/l goes to the next stage. According to the test, this part of the water can reach a temperature of 60 °C. And with the process of evaporation and condensation the salt water is also transferred into fresh water and been collected in the container. According to the previous study, when only the first stage of the distiller is adopted, the efficiency is around 45%. In order to find out in what extent the performance of this device can be reached by applying the two-stage technology, some experiments were conducted.

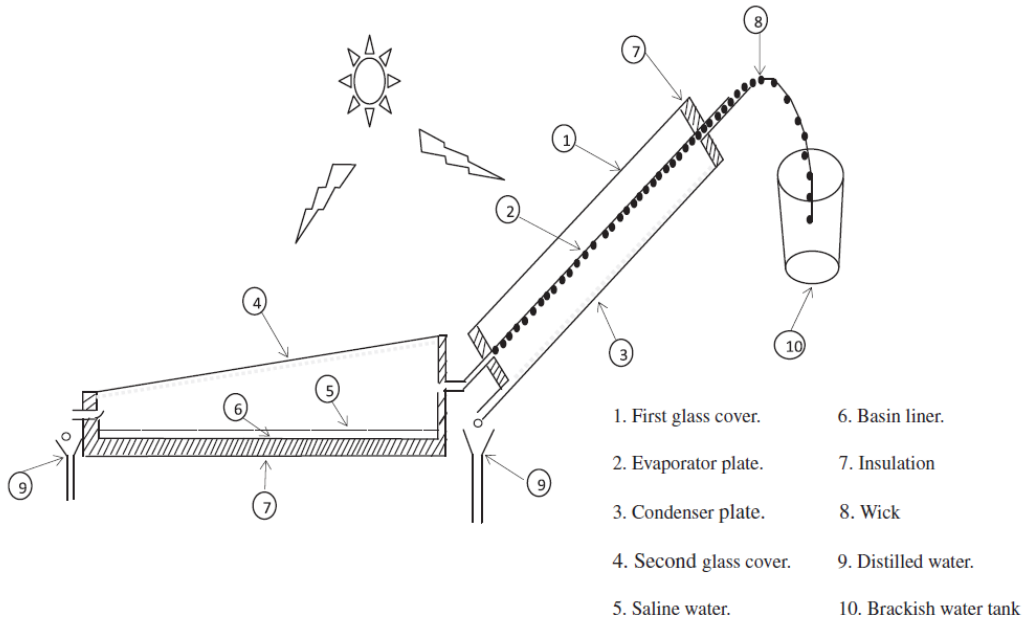

Fig. 1.4 Schematic diagram of a new combination solar passive distiller[10]. (Picture taken from Ref.[10], with permissions)

From the experiment data, for sure the new passive solar distiller has a higher productivity than any one single stage when applied in the same situation. Moreover, the key point that can change the performance of this desalination device is the ratio between the area of the basin in the second stage and the area of the evaporator. When the ratio increases in a reasonable range the fresh water productivity will increase in response. Besides, another thing is that the best performance of this device can be

reached when the first stage is set to have an angle of 32° with respect to the horizontal direction. All in all, this device did the combination of two type of devices in the first time and this remarkably increase the efficiency of the passive solar distiller. However, the problem of clogging is still not solved and for sure the performance of this device will be worse and worse without maintenance.

The performance analysis of modified basin type double slope multi–wick solar still device has been discussed by Piyush Pal and his co-workers in 2017[13]. The structure of the optimized passive solar distiller with double slope is demonstrated in Fig. 1.5 (Picture taken from Ref.[13], with permissions). Like the conventional solar still, this device can be divided in three parts from the top to the bottom. The first important part in this passage is the top part which is composed of two glass covers in double slope shape and four transparent walls in four directions. In order to make sure that when the vapor touches the glass plate, the distilled water remains adhering to the plate, and also the salt water can be risen up to the top by the wick easily, the slope of these two covers should not be set too steep. Another thing needed to be focused on is that the size of the glass cover should not be too large. For these reasons the two glass covers are set with an angle of 15° inclined with respect to the horizontal direction. Since this part is the key part to ensure that the maximum heat energy of the sun can be conducted to the basin, the material and the size of the walls should be mainly focused on. Here two types of materials are applied on four walls (Fiber Reinforced Plastics and acrylic), and there's also an equivalent transformation in terms of the thickness when the same heat transfer rate is considered, that is 3mm of the acrylic is equal to 5mm of the Fiber Reinforced Plastics. This relationship is derived from the Fourier's law of heat conduction:

$$Q_{Cond} = K_{FRP} \times A_{FRP} \times \left(\frac{T_2 - T_1}{L_{FRP}}\right) = K_{ACRY} \times A_{ACRY} \times \left(\frac{T_2 - T_1}{L_{ACRY}}\right)$$

Where Q_{Cond} is the amount of heat transferred under a specific condition, $K_{FRP} = 0.351W/(m \times K)$ and $K_{ACRY} = 0.2W/(m \times K)$ are the thermal conductivities of Fiber Reinforced Plastic and acrylic respectively. T_1 and T_2 are temperature of the two sides of the Fiber Reinforced Plastic plate. And L_{FRP} and L_{ACRY} are the thickness of the Fiber Reinforced Plastic and the acrylic plate. Thus, when $L_{FRP} = 5mm$,

$$L_{ACRY} = \left(\frac{K_{ACRY} \times L_{FRP}}{K_{FRP}}\right) = 2.85mm \approx 3mm$$

In this case, two plates with 3mm thickness of the acrylic and also an area of 0.12m^2 (1 m with length and 0.12m with height) are applied on the east and west walls. Another acrylic plate with the same thickness but different size (2m with length and 0.12m with height) is used as the south wall. The only wall left (the north wall) is made of Fiber Reinforced Plastic with a 5mm thickness and the size is the same as the south wall. As for the salt water container, the black Fiber Reinforced Plastic with a thickness of 5mm is applied to improve the probability that the solar heat energy reaching the basin so as to increase the rate of evaporation.

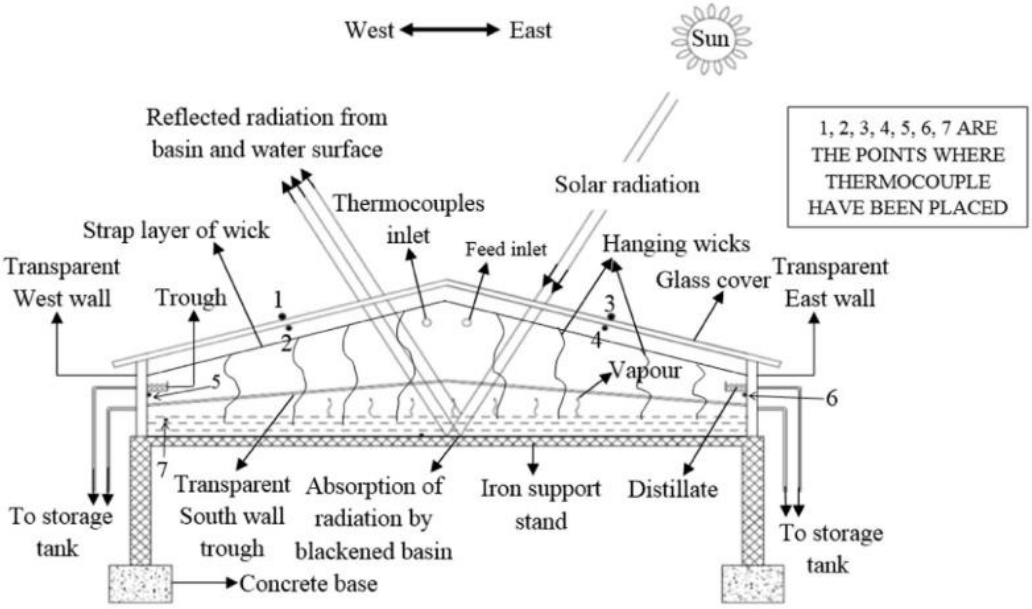

Fig. 1.5 Schematic diagram of double slope shaped multi–wick passive distiller**[13]**. (Picture taken from Ref.[13], with permissions)

The last part of the device is the collection system which consists of the storage tank and the plate on both west and east sides. In order to make sure that the salt water and the fresh water will not be mixed, the plate should keep a distance with both the upper (distilled water) and the lower side (salt water). There are also four plastic pipes on each direction between the tank and the collection plate. The inlet is used to fill the basin with salt water during the operation. The model of the passive solar distiller for experiments is demonstrated in Fig. 1.6 (Picture taken from Ref.[13], with permissions).

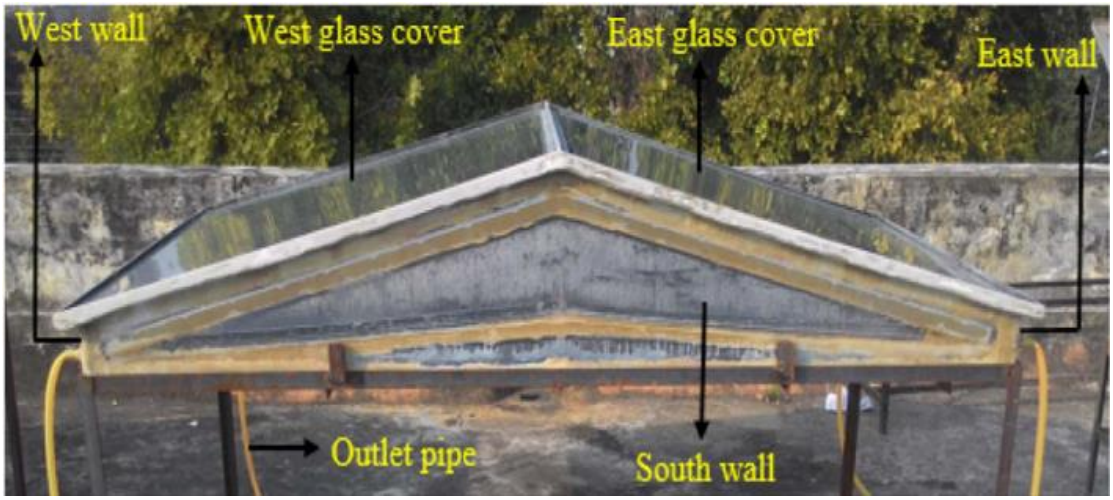

Fig. 1.6 Photograph of the model of the passive distiller **[13]**. (Picture taken from Ref.[13], with permissions)

The working principle is like this, from the beginning, due to the gravity, the salt water is supplied into the basin through a pipe connected the inlet on the front wall which is then absorbed by the wick and sent to the top layer of wick (made of jute or cotton) owing to the capillary forces. Afterwards, due to the heat energy provided by the solar radiation, the salt water is vaporized during the day time. Then the vapor starts moving randomly in the space of the distiller and when it touches the inclined glass covers and

the upper part of the transparent walls whose temperature are relatively lower than the vapor, it will be condensed into small droplet and flow down to the collection plate and then into the storage tank. After the whole process, the salt water is purified into drinkable fresh water which is free of insalubrious substances for human beings like microbiological organisms and heavy metal. Due to the opacity of the walls on four sides, the previous traditional solar distiller could not effectively use the solar energy during sunset and sunrise, but only waited for the inclined surface of the distiller to be exposed to the sun when the sun rose to a certain angle so that the salt water in the container is under radiation, being heated and evaporated. The improved solar distiller can heat the salt water in the container and the salt water in the wick layer at the same time, which also improves the overall efficiency and realizes an increase in the output of fresh water.

Before the experiment, in order to have an accurate data, the solar distiller must be cleaned and the salt water should also be in an appropriate level of the basin before the sun goes up. Moreover, some other compulsory data needed to calculate the final result are required at each hour during one day, like the solar intensity, the temperature of the salt water container and some other points of the device, and most important the amount of distilled water in the tank.

To make a conclusion, this study does more optimization methods with respect to the previous one. On the one side, this device can be seen as another type of combination of the conventional solar distiller and the wick-based passive distiller (in a up and down form but not a two-stage one), thus, not only the salt water in basin but also the salt one absorbed by the wick are under the sun illumination, which increase the rate of the evaporation of the salt water. On another side, the Fiber Reinforced Plastics and the acrylic material are applied on the solar passive distiller for the first time. Especially the side walls are transparent, which increase the solar energy absorption ability of the whole device. Thus, with longer time of sun illumination, the more water will be heated up and vaporized. This helps improving the performance of the device with effective evaporation. These two optimization methods together lead to the growth of the productivity of the fresh water. However, like other technologies talked in the previous passage, this device also needs the maintenance regularly, the basin and the glass cover need to be cleaned, for example, sediments like salts, sand and some other microbiological organisms.

In accordance with all the cases talked in previous text, although with good performance in terms of fresh water productivity, a severe problem is still not solved by these technologies–how to keep the performance stable during a long-time operation. Actually, the principle of all types of the solar passive distiller is the same, the liquid salt water is vaporized and then condensed. In this procedure, the solid as salt will be left and accumulated on the evaporator, thus clogging the device and then the performance of the device is affected[15, 16]. In order to breakthrough this barrier, some other devices and technologies have been discussed in literatures.

In 2017, Varun Kashyap and co-workers report a new efficient and flexible material structure for solar-desalination with anti-clogging characteristics[12]. The structure of the material is quite unique, it’s composed of three other materials, the main supporting

frame is made of polymer, and the rest of the space is taken by the combination of carbon fibers and flake-shaped graphite. The procedure to construct the material is shown in Fig. 1.7.

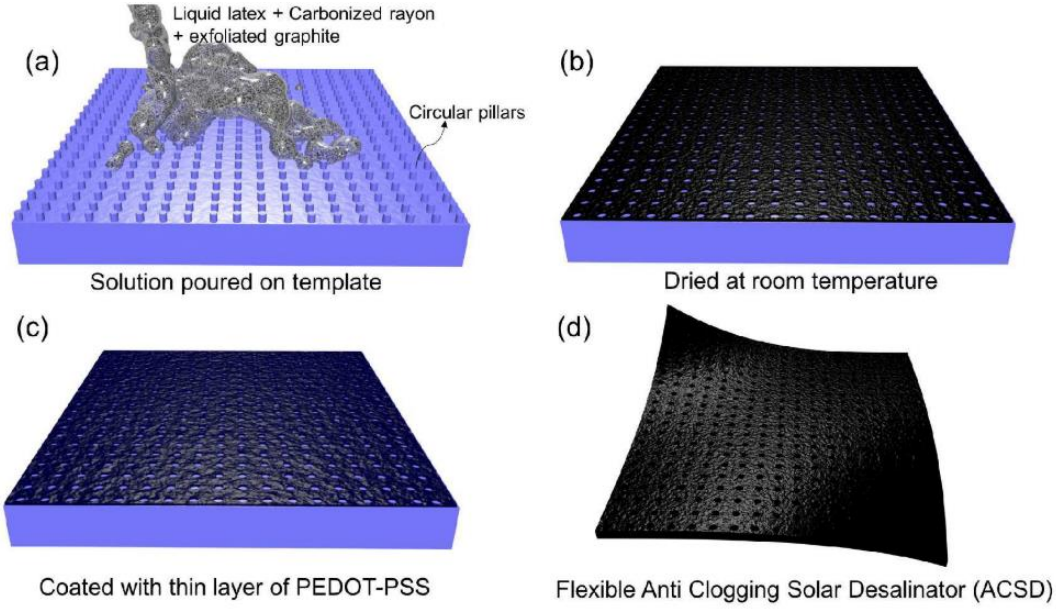

Fig. 1.7 the procedure to construct the material[12] (Picture taken from Ref.[12], with permissions)

For the reason of this unique porous structure, the salt is not allowed being accumulated on the surface of the material. The working process is like this: when the material is put in the basin as the evaporator, the salt water will be risen up by the capillary action, during the evaporation process, the solid salt will be separated out. However, because of the presence of the PEDOT-PSS, the salt particles are not allowed to stick on the surface. Besides, the size of the pores is designed as the channel for the salt particles to back to the salt basin due to the gravity. After several experiments in both the laboratory and the environment, results show that the performance of the solar passive distiller equipped with this material is very stable even with a high salt concentration liquid. Thus, this type of material with simple but unique structure can be applied in most solar distiller and help maintain the good productivity of fresh water. Soon afterwards, a special 3D cup-shaped solar evaporator is fabricated by Shi and co-workers which can achieve Zero Liquid Discharge (ZLD) desalination[20]. The principle behind this is that, unlike the conventional evaporator with just 2D dimension, this evaporator with a third dimension which is mainly used for salt accumulation while the horizontal evaporator will not be affected by salt articles. In this way, the two parts of the evaporator are smartly separately separated and each one has its own specific function. However, these materials may not the best solution to solve the clotting problem under the condition of emergent conditions. Because some of them are not easy to get and also expensive.

In 2020, an important proposal in dealing with the clogging problem was given by Jiale Xu and co-workers[18]. They demonstrate a strategy to address the salt fouling issue for the solar-driven interfacial evaporator (SIE)-based solar still (see Fig. 1.8,). This device allows to separate from solid salt and collect these two matters at the same time. The main principle behind this technology is that by controlling the concentration gradient of the salt water which is absorbed by a specific layer of printed paper. And

this will lead to the localized surface salt precipitation around the boundary of the evaporator. According to the experiment results, this device has the ability of keeping a high efficiency (~78%) during long-term operation, and this performance is also very stable by applying the localized surface salt precipitation technology. Besides, this technology is suitable not only for high but also low salt concentration fluid, for example, a good transformation rate of 40.3% can be reached with only 10 wt.% salt solutions. One other point worth emphasizing that this technology makes it easier for the collection of solid salts, but without complex process to product and purify the salt adopted in conventional salt industry. And the productivity of the salt can be reached at 0.42 kg m^{-2} day^{-1}, which is quite efficient. A part from this, all materials and components applied on this device are cheap and can be easily found in the market. For all those points talked about, the LSSP-based passive solar distiller offers a new stable way to provide fresh water supply and also salt in areas with little fresh water resources.

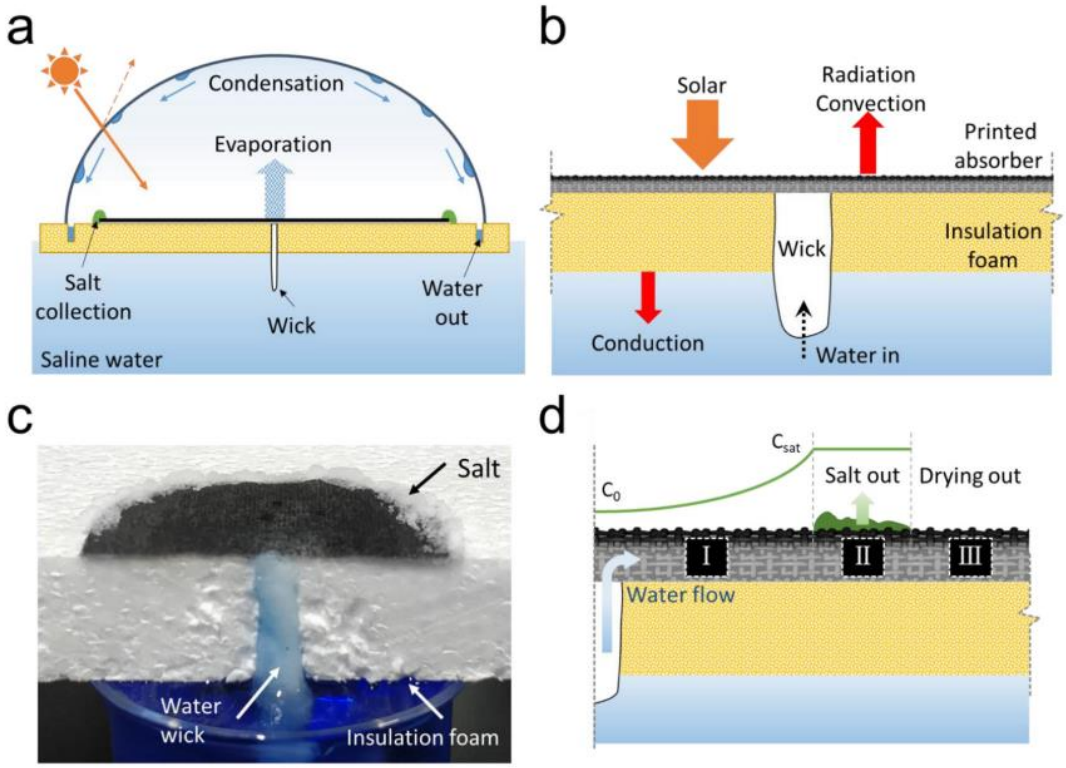

Fig. 1.8 The schematic structure of the solar passive distiller with localized surface salt precipitation design. (a) Overall structure of the desalination device. (b) Demonstration of energy balance and flow of matters exchange happened on the evaporator of the passive distiller. (c) The demonstration of the capillary action during the experiment. The salt water (blue liquid) is absorbed to the evaporator by the wick. (d) The process of the change of the concentration of the salt water after being risen up on the evaporator and the localized salt precipitation phenomenon. (Picture taken from Ref.[18], with permissions)

Unlike other types of passive solar distiller with a salt water basin, this device is designed to be able to float on the seawater. The structure is mainly composed of four components, the transparent plastic cover, the evaporator layer, the insulation foam and the wick. From the start, the salt water is transported to the hydrophilic layer for the reason of the capillary action provided by the cotton wick, and then fill the whole layer

during diffusion. Thanks to the presence of the cylinder-shaped transparent cover on the top and the dark colored surface of the evaporator layer, the heat energy of the sunlight can easily be absorbed by the salt water, which leads to a high kinetic energy of water molecules. These molecules move randomly and go out from the liquid. When they met the inner surface of the plastic cover on the top and side, because the temperature difference between them, the vapor is then condensed into small droplet and flows along the cover and is collected by the collection system in the end. In the meantime, because the salt concentration is lower near the wick (sea water) but high near the edge of the evaporator, the salt will come out firstly on the edge area. And also because the concentration difference, the salt water will keep moving from the center part to the edge area, which means the performance will not be affected by the clogging problem and is able to perform stably for a long period. The insulation form is made of polystyrene material which is able to conduct the heat that is not absorbed by the salt water in the evaporator to the sea. Also, because the light-weight of the material, the whole device can float on the sea by itself.

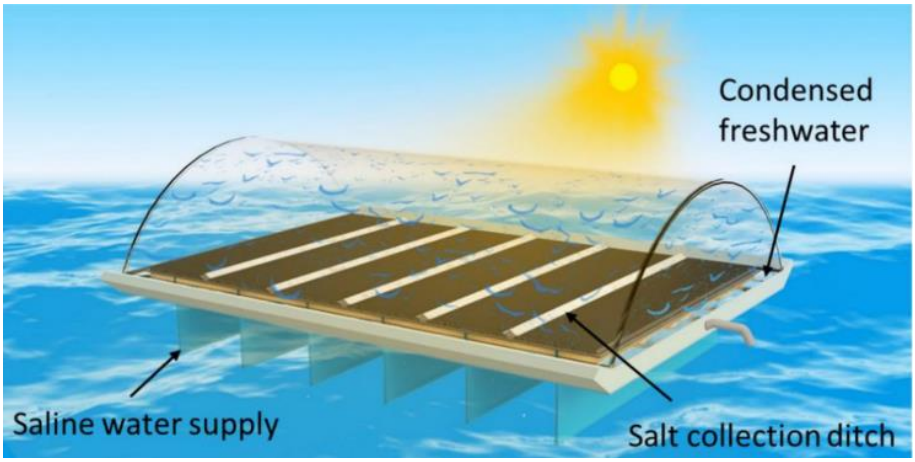

Fig. 1.9 Optimized solar passive distiller device which can achieve salt harvest in the meantime.[18] (Picture taken from Ref.[18], with permissions)

From what has been discussed above, the optimized solar passive device based on LSSP solves the fouling problem and also provides a chance to collect the salt. The self-floating of this device also simplify the process and equipment needed to produce fresh water. However, this device needs someone to collect the salt after a certain period, otherwise the space for evaporation will be smaller and smaller and the efficiency will be affected. thus, it's still not a good solution.

In the same year a salt-rejecting floating solar still for low-cost desalination was proposed by George Ni and co-workers[14]. In their passage, an optimized solar passive distiller which is free from the fouling problem is fabricated. According to the experiment data, this device shows a significant salt rejection rate during the operation, which helps keep a stable supply of fresh water in a day without regular maintenance and cleaning of the device. And the productivity of this device can reach about 2.5 L m^{-2} day^{-1} which is enough for an adult to drink with the solar-water efficiency of around 22%.

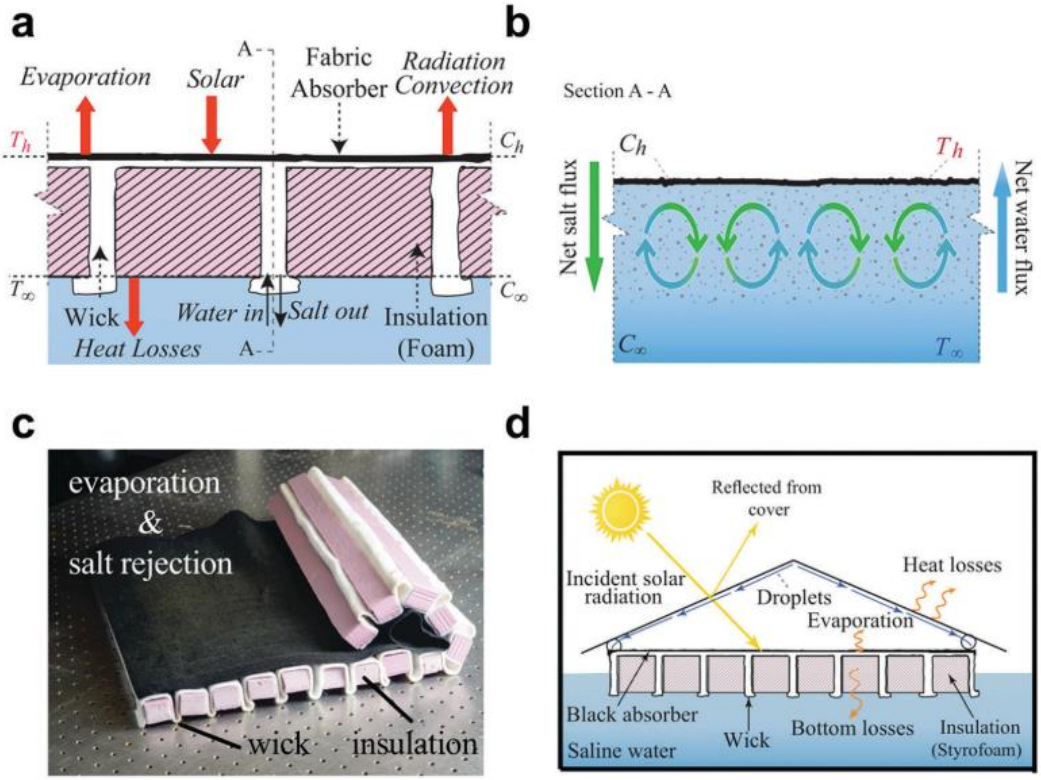

Fig. 1.10 An optimized fouling-free solar passive distiller structure. (a) The detailed structure of the solar passive distiller, the insulation foam is made of polystyrene, the evaporator is painted black to increase the solar energy absorbed, the wick is used as the channel for salt water to go up and also the salt to back to the sea. (b) The flow process of salt water and salt particles during the operation. (c) Real model of evaporator fabricated for the experiment. (d) Schematic diagram of the solar passive distiller in the ocean and the energy balance and the transport of matters. (Picture taken from Ref.[14], with permissions)

Another important improvement of the device is that, unlike conventional solar distiller with glass covers and walls, the lighter and cheaper polymeric materials are applied on the cover and all the skeleton. In this way, the solar passive distiller can realize self-floating on the sea and this saves costs for basin and other equipment. Fig. 1.10 gives detailed information about how the self-floating solar passive distiller which is able to reject salt back water is constructed. The double slop shaped covers made of lightweight polymeric material are installed on the top of the device. Apart from the character of high light transmittance and heat insulation ability to ensure that more heat energy can reach the evaporator and prevent heat losses, the component also is also adopted as the condenser. Thus, the thermal conductivity of covers must be as low as possible. The lower part of the device constitutes of evaporation layer and insulation material. The heat energy of the solar radiation is absorbed by the upper layer of the evaporator, for this reason, the cellulose fabric used is painted into black (Fig. 1.10c). Beneath it is the white porous material, the wick, whose function is to take the salt water up and be filled with the salt water so that the thin layer of water can be heated and evaporated in a short time. And because of the porous structure of the wick, it also enables the salt particles going back into the ocean. Between each wick material there is the insulating material which is the key component to make sure that the heat of the evaporation layer is not

conducted to the water thus reducing the amount of vaporized water. Consequently, a low thermal conductivity material (polystyrene foam) is applied on this component. In fact, here are mainly two elements very important for the performance of the solar passive distiller. From the energy point of view, there should be as much heat energy as possible being absorbed by the system and also little leakage of this energy. This is realized by the cover and the insulating layer. From the salt rejection rate point of view, there should be as many channels as possible so that the precipitated salt particles could be sent down in to the ocean timely, which means there should be more wicks. However, the wick is not thermal-insulating, thus it's very important for this system to reach a balance between the percentage of the wick and the insulating materials. Here a critical ratio is considered to decide the overall performance of the distiller, that is the ratio between the fabric wick area and the aera for insulation. Obviously, this type of solar passive self-floating distiller paves a way for satisfying the fresh water needs for residents in island area with its robust structure, cheap materials and stable performance in long-term operation. However, no theoretical principle behind the salt rejection was explained in this study, but only a few words about diffusion and convection, this prevents to rationalize and generalize the methods applied in this passage.

Furthermore, Zhenyuan Xu and co-workers[19] present a type of thermally-localized multistage solar still (TMSS) which enables high-efficiency low-cost desalination. Fig. 1.11 gives information about the structure of the thermally-localized multistage solar still. The thermally-localized multistage solar still is composed of several stages and each stage the same configuration except the first and the last stage. As for the first stage whose main function is to convert the solar irradiation in to the heat energy for the whole system and also do the first step salt water distillation, the selection of the absorber is very important. The material must have a very low thermal-conductivity keep a high temperature to evaporate the water[21-23]. The silica aerogel can not only provide a high transmittance but also thermal insulation and physical protection for the solar absorber. In order to keep a large temperature difference of previous stages and the last stage which promotes the vapor going forward towards the last stage, the condenser is immersed in the sea water. For each stage, the sea water is risen up by the wick layer through capillary forces and then is vaporized by the solar heat (the first stage) or the latent heat released by the previous stages (through condensation). The vapor is condensed into drinkable water when it contacts with the surface of the condensing plate. The fresh water is collected by the external container. There are mainly three points behind the thermally-localized multistage solar still to explain why the performance of this device is better with respect to other types of solar passive distiller. The first reason is that the whole system is set in a vertical way, so that the surface of the solar absorber can be adjusted towards the sunlight whenever it is, which means the energy of the solar radiation is fully utilized in the daytime, in addition, this configuration allows quite a large distance between the evaporator and the ocean, which prevents the heat losses. Secondly, the separation design of the solar absorber and the wick layer is also good for the improvement of the performance of the solar passive distiller. The reason is that the solar absorber is only responsible of the solar energy intaking, and the wick layer is only used for rising up salt water, which means the best

performance of energy absorbing and capillary effect can be simultaneously achieved when the most suitable materials for the two functions are applied. This solution is much easier and cheaper than find a material which is qualified of two functions at the same time. Finally, the application of the multistage arrangement of the distiller can realize the energy of the vaporization (latent heat) which is released by the front stages being utilized by the stages behind, which also increases the efficiency. Of course, there are also some other parameters like the thickness of each layer, the distance between every stage and the width of the device which also play important rules on the performance of the device.

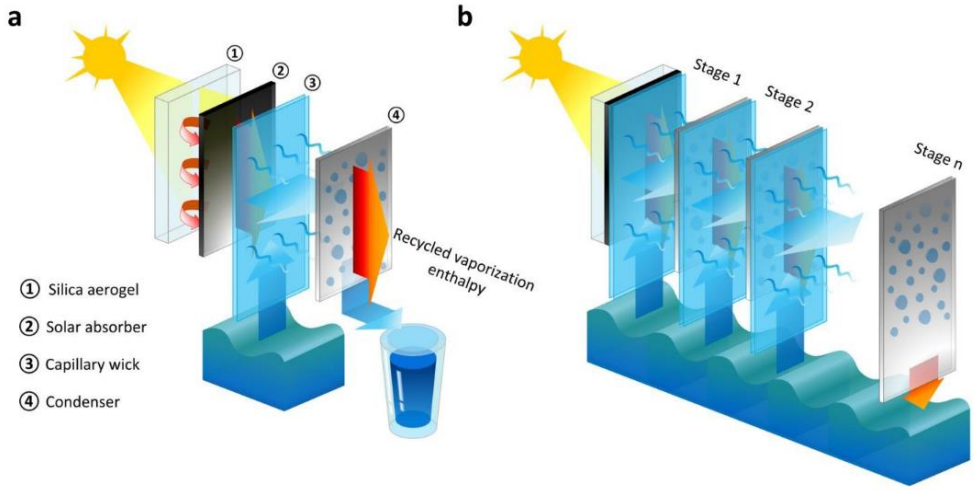

Fig. 1.11 Schematic diagram of the thermally-localized multistage solar still configuration. (a) The composition of the thermally-localized multistage solar still. The first stage is composed of a silica aerogel layer whose function is to allow as much the solar energy as possible to get in and thermal insulation, a solar absorber to transfer the solar energy into heat, the capillary wick layer to wick up salt water and evaporate the liquid into vapor, the condenser to condense the vapor. And there is a collection system to collect the fresh water from each stage. (b) How the energy is recycled by the thermally-localized multistage solar still. The energy (latent heat from the condensation) released by the previous stages is utilized by the next stages. The condenser of the final one is immersed in the salt water to keep a large temperature difference between the evaporator and the condenser. (Picture taken from Ref.[19], with permissions)

Through some experiments, the main barrier to the improvement of the performance is how to increase the utilization of the solar energy and the mass transportation. There are several parameters that can significantly improve these two parameters, like the thickness of each layer, the distance between every stage, the width of the device and the number of stages. Finally, the optimized ten-stage thermally-localized multistage solar still is designed and tested in both laboratory and the real environment whose efficiency can reach 385% and the production of the fresh water is about 5.78 L m^{-2} h^{-1}, which is quite good. But like in Ni's study, they also cannot explain the basic reason of the high salt rejection rate of this device.

In this work, based on the study of Matteo Morciano and co-workers[24], a type of existing optimized solar passive distiller which has been experimentally tested is

discussed. Apart from the geometry and configuration of the device, the working principle and process is also discussed. The most important subject of this passage is the theory behind the good performance in terms of salt rejection of this device, and the conclusion is confirmed by simulation in COMSOL Multiphysics. The key result lies in correlating the Marangoni effect[25] which happens at the water-air interface, with effect salt removal. The principle is like this, when there is a temperature difference or concentration difference between two sides of the liquid, there will be a surface tension in response, this shear stress will drive the fluid flowing from the low shear stress part towards the high shear stress part.[26] As a result, the salt particles will be removed by the driven force automatically an there will be no salt accumulation and fouling of the evaporator. This process is also seen in many procedures like welding[27], electron beam melting[28] and crystal growth[29], Although in many literatures [30] the Marangoni effect is investigated and discussed , it has never been considered to be a key contribution in the region of salt rejection and desalination. Thus, this work mainly explores how the Marangoni effect happening during the operation of the solar passive distiller and how some parameters (like concentration gradient and the thickness of the evaporation layer) can have an effect on the performance of the salt rejection rate by using the software COMSOL Multiphysics.

2. Protocol and methodology

2.1. Device and working principle

In this work, in order to show clearly the optimization process of the hydrophilic layer (evaporation layer), first thing is to introduce the existing device which has been experimentally tested.

The solar passive distiller is a device which is able to transform saltwater to freshwater without using other type of energy but only solar energy. The working process and the detailed structure are demonstrated in Fig. 2.1.

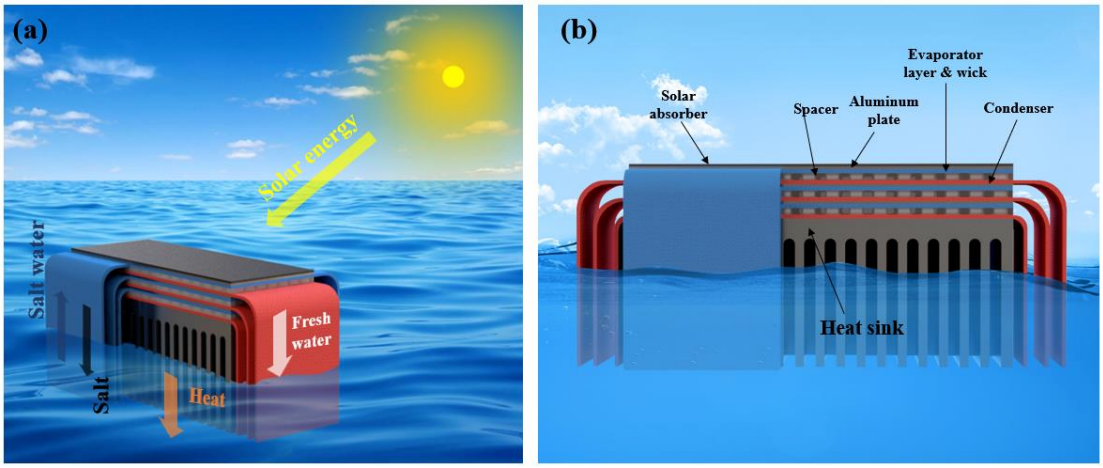

Fig. 2.1 The working process and the structure of the 3-stage solar passive distiller. (a) conceptual model of the device (b) detail of the configuration of each component of the device.

This solar passive distiller is composed of three stages. And there is an aluminum layer with a thickness of 1mm and an area of 12 × 3.5 cm^2 installed between each stage, the aluminum plat has good conductivity of heat so that the heat energy from the solar absorber (for the first stage) and the latent heat from the previous condensation procedure (for the next two stages) can be utilized for the evaporation process and these aluminum plates also provide support and robustness for the whole device. On the top surface of the device there is an aerosol-based solar absorber which is made of aluminum and painted in black with Zynolyter Hi-Temp material which processes a good thermal property. The function of this component is to absorb the solar irradiation and convert it into the heat energy in an effective way. For the first stage, the first layer is the evaporation layer (the blue one) which is made of fiber-based wick material (Sungbocleamy) which can pump the salt water up on the horizontal surface with a height of 5.5cm in the test, which is enough for the 3-stage passive distiller due to capillary action. Then here is a Plexiglass frame made of linear low-density polyethylene which is used as an air gap (see Fig. 2.3) between the evaporator and the condenser (the red one) whose function is to create a sufficient space for the evaporator and the aluminum plate so that to keep a temperature difference between two layers and that the salt water and the distillate fresh water are not mixed. Also because of the porous structure of the component, the possibility of the salt accumulation and the

fouling problem on the evaporator and the metal plate can be decreased. The condenser is used to turn the vapor from the evaporator into the liquid to collect. The next two stages are the same configuration (composed of an evaporator and a condenser). Under the last stage there is a heat sink which is immersed in the sea water and this helps release the heat to the water and thus keeping a sufficient low temperature of the condenser of the last stage to keep a vapor difference which drives the vapor flowing from the evaporator to the condenser.

From the start, the salt water (deep blue arrow) in the sea is risen up to the horizontal plain of the evaporator of every stage by the vertical portion on the two sides through capillary force. Then, the black solar absorber installed on the top surface of the distiller converts the sunlight (yellow arrow) into heat energy which heats the salt water up in the evaporator. The high temperature evaporates the liquid into vapor which then flows into the condenser because of the temperature difference between the evaporator and the condenser layer. After that, the vapor is condensed when it touches the condenser and the fresh water (white arrow) flows along the vertical part of the condenser because of the existence of gravity and then can be collected. The black arrow is to show the net flow which is driven by the Marangoni effect. (See Fig. 2.3)

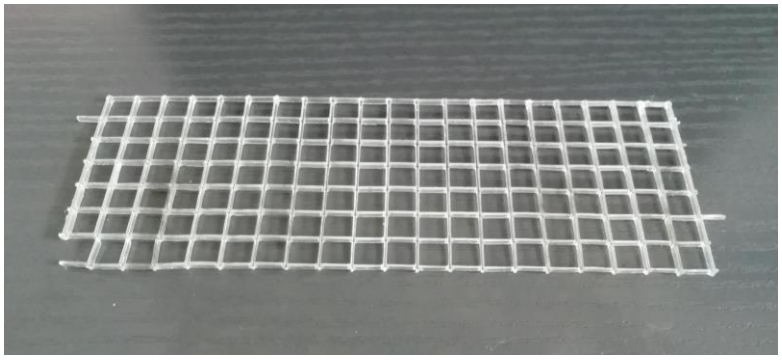

Fig. 2.2 detail of the shape of the air spacer.

In conclusion, the optimized solar passive distiller realizes a good performance in terms of the salt water distillation. Firstly, the solar absorber and the evaporator are decoupled, which is good for choosing the most suitable material for two functions. Moreover, the multistage configuration realizes a high efficiency of heat energy utilization because the latent heat of the previous stage can be applied by the next stage. Then, with the increasing area (with a length of 12cm) of the vertical portion of the evaporator layer, there is more possibility for the salt to be carried out of the device by the Marangoni flow. Besides, since the width of the evaporator is just 3.5cm, the longest path out the horizontal surface for the net salt flow is just 1.75cm. Then, unlike the traditional structure of the solar distiller, the condensed droplets will not degrade the optical performance of the solar absorber. Finally, and also the most important one, this device provides the principle of how to reject salt and prevent fouling problem during operation, and this paves a way for improving the salt rejection performance in the future. However, here are some parameters which is related to the performance of the distiller that needed to be focused. For example, the material used for evaporator should have a good wicking ability, the thickness and the permeability of the air gap should be in the most suitable situation and the thickness of the evaporator is very important for

the Marangoni effect and thus salt rejection. In order to explore how the thickness and also the initial value of salt concentration on the left side of the evaporator can have an effect on the salt rejection performance, several numerical simulations are conducted by using COMSOL Multiphysics.

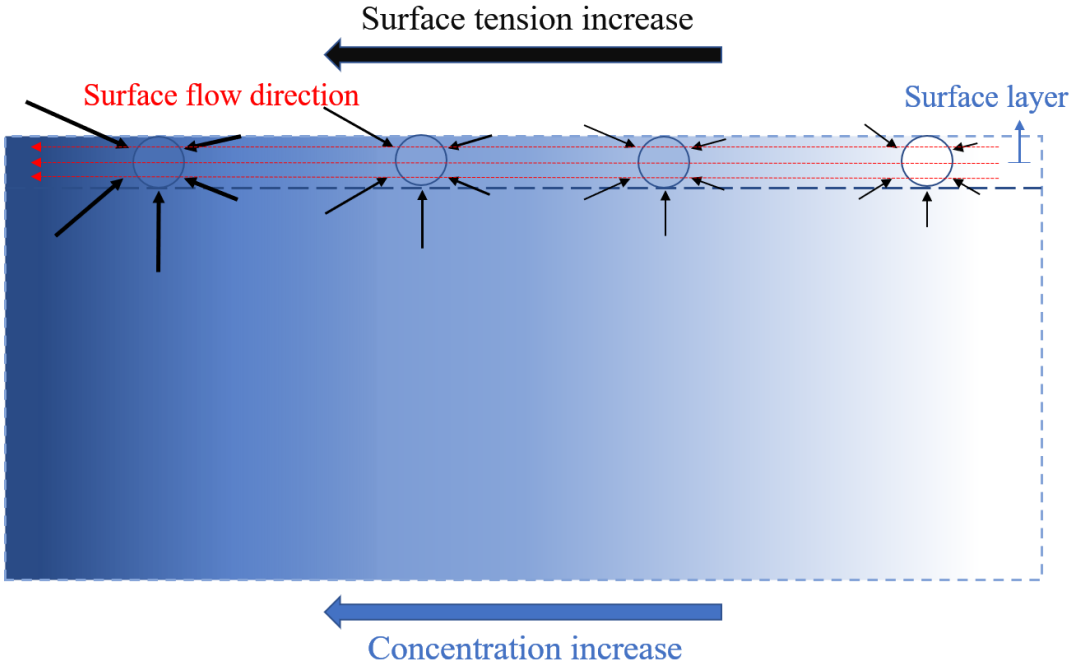

Fig. 2.3 Demonstration of the Marangoni effect. The change of the salt concentration can also induce a change of the surface tension. Because of the surface tension gradient, there is asymmetric interactions among water molecules Thus, there will be a flow from low surface tension area towards high surface tension area near the surface.

2.2. Numerical simulation

In this work, the study mainly focus on the section of the evaporator layer which consists of a saltwater thin film (namely the hydrophilic layer, see Fig. 2.4). And the optimization process of it.

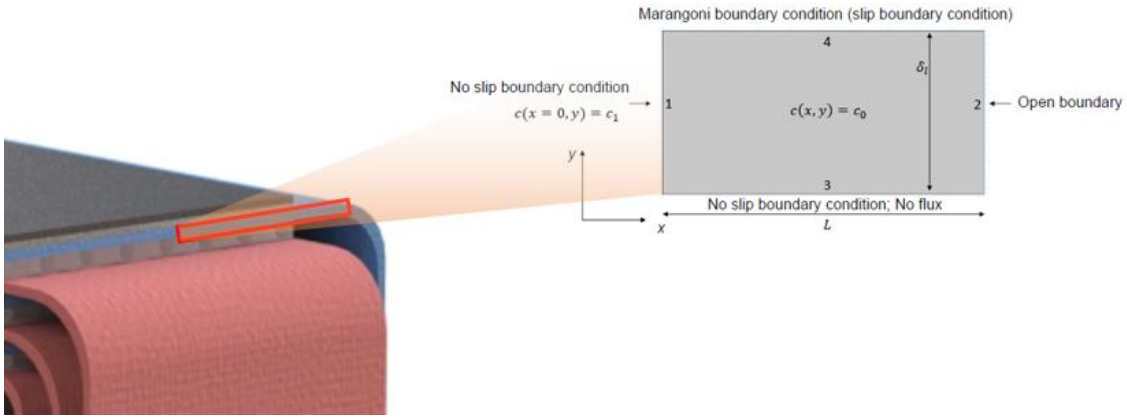

Fig. 2.4 The evaporator layer domain to be simulated

In order to start a simulation, the first step is to build a model by using either the component function or other modelling software and input it in the COMSOL. Here we

draw a rectangle as in Fig. 2.4 to be the simulation domain which gives information about the thickness σ (y-direction) and the length L (x-direction) of the evaporator. In our study the thickness is range from 0.5mm to 5mm. The length is equal to 17.5mm. The next step is to define the material of the domain. Here the domain is consisting of the saltwater, the dynamic viscosity $\mu = 1 \times 10^{-3} Pa \cdot s$ and since the concentration of the salt water keeps changing during the process, the density also changes. The relation between the density and the concentration is as follow:

$$\rho = \rho_0(1 + \gamma c) \tag{1}$$

Where $\rho_0 = 1045\ kg\ m^{-3}$ is the fresh water density and $\gamma = \frac{\rho_s - \rho_0}{c_s - c_0}$ is the proportionality constant between concentration and density. c_0 and c_s are the salt concentrations of the fresh water (namely $0\ mol\ m^{-3}$) and saturated salt water ($4480\ mol\ m^{-3}$). $\rho_s = 1164\ kg\ m^{-3}$ is the density of the saturated salt water. Then, we should add the physics phenomenon that are related to our study. Here we need to couple the laminar flow and the transport of diluted species to investigate the advection–diffusion phenomenon in presence of an interface with varying salt concentration gradient and different thickness. And the simulations are performed under transient condition. The equation of the transport of diluted species is expressed as this:

$$\frac{\partial c_i}{\partial t} + \nabla \cdot (-D_i \nabla c_i) + \mathbf{u} \cdot \nabla c_i = 0 \tag{2}$$

Where c_i is the concentration of species i, here it's the salt in the sea water, D_i is the molecular diffusion coefficient and $D \approx 1.5 \times 10^{-9} m^2 s^{-1}$.[31]

In the section of the transport of diluted species we also need to set the boundary condition in Fig. 2.5. In detail, the no flux condition is applied on boundary 3 (since in the problem we study no mass flux is considered through the side walls), of which the equation is like:

$$-\mathbf{n} \cdot (-D_i \nabla c_i + \mathbf{u} c_i) = 0 \tag{3}$$

About the initial value, we set the entire domain to be the sea water concentration, namely $c_0 = 600\ mol\ m^{-3}$ (since the evaporation layer is immersed in sea water which is risen up by the capillary force at the beginning). Then the concentration of the left boundary (namely boundary 1) c_1 is set to be a Dirichlet boundary condition to model an arbitrary fixed salt concentration during the real salt rejection process. The last setting of this is that the right boundary (namely boundary 4) should be in open boundary condition, since it's the exit of the mass flux. The equation is expressed as:

$$-\mathbf{n} \cdot (-D_i \nabla c_i) = 0, if\ \mathbf{u} \cdot \mathbf{n} \geq 0 \tag{4}$$

$$c = c_0, if\ \mathbf{u} \cdot \mathbf{n} < 0 \tag{5}$$

Moreover, the exterior concentration of this boundary should be the same as the sea water concentration, that is $c_{0,c} = 600\ mol\ m^{-3}$.

In terms of the laminar flow, the Navier-Stokes equation momentum equation is applied:

$$\frac{\partial \rho \mathbf{u}}{\partial t} + \mathbf{u} \cdot \nabla(\rho \mathbf{u}) = -\nabla p + \nabla \cdot (\mu(\nabla \mathbf{u} + (\nabla \mathbf{u})^T) - \frac{2}{3}\mu(\nabla \cdot \mathbf{u})\mathbf{I}) \tag{6}$$

Where ρ is the density of the fluid (see equation (1)), and $\mathbf{u}$, μ is the velocity and the viscosity of the fluid, p is the pressure. As for the boundary condition of this part, we

should set boundary 1 and 3 to be the no slip boundary condition (namely $\mathbf{u} = 0$ and the equation is the same as (4) and (5)), because these two boundaries of the evaporator layer have contacts with the Aluminum plate which is a not moving wall. Whereas the boundary 4 should be under slip boundary condition to model the velocity introduced by the concentration gradient, which is the so-called Marangoni effect. The equation is like this:

$$[-p\mathbf{I} + \mu(\nabla\mathbf{u} + (\nabla\mathbf{u})^T) - \frac{2}{3}\mu(\nabla \cdot \mathbf{u})\mathbf{I})]\mathbf{n} = \sigma\nabla c \quad (7)$$

In this equation, $\sigma = \frac{\partial\gamma}{\partial c} \approx 1.89 \times 10^{-6} \frac{N\,m^{-1}}{mol\,m^{-3}}$ [32, 33]is the concentration derivative of the tension. Finally, the outlet is applied on the boundary labeled with 2 and the pressure is set to be 1 atm.

Since our study is based on finite element method (FEM), the set of mesh is very important to get a convergent outcome. Here we must obey the Courant–Friedrichs–Lewy condition. As a consequence, the time step must be less than a certain time in many explicit time-marching computer simulations, otherwise the simulation produces incorrect results. However, we also cannot use too much mesh, otherwise, we will have a huge computation cost, which waists a lot of time. So, our mission is to find a balance between the accuracy and the computing time.

There are many ways in COMSOL to build the mesh, the mesh can be automatically built by the software itself according to our geometry and the physics we focus on. We can also set it by ourselves, and this way we often can have a better result with less mesh, which means more efficient.

In this study the mapped mesh is applied on x and y direction. And since the velocity is smaller on the left side, we set a separate point near the left boundary so that we can have finer mesh in this part. During the simulation process, we also need to change the mesh setting according to the concentration gradient and also the thickness of the evaporator layer. Finally, the main criterion to decide whether the mesh is good or not is to plot the molar flux out the right boundary and to see if the plot reaches a stable state after a certain period.

Also, the plot of velocity is needed at several distance away from the left boundary and these results should be compared with the purely diffusive flow situation to get the final conclusion.

3. Results and discussions

In order to figure out how the Marangoni effect is related to the salt rejection phenomenon the numerical simulation is needed to investigate how the concentration changes in Marangoni effect condition and in pure diffusion condition respectively. According to the simulation result, the main reason that the fouling and salt accumulation is not happened on the horizontal surface of the evaporator during operation is the enhanced flow and mass transport caused by the Marangoni effect. Near the air-water interface, the difference of surface tension in two sides will induce a localized viscous stress which pushes water molecules flowing towards a specific direction. Generally speaking, this surface tension gradient is induced by the concentration gradient or the temperature gradient (also known as thermo-capillary convection) of the liquid. In this study, the Marangoni effect is caused by the concentration gradient of salt in two ends of the domain. The higher concentration is the salt water the larger the surface tension is, which means the flow is from the low concentration area to the high concentration area. Considering that the up (labeled as 4 in Fig. 2.4) and down (labeled as 3 in Fig. 2.4) boundary of the domain is contact with the aluminum plate and air-spacer respectively, there will be no convection there, thus, the only outlet for the flow is the right boundary (labeled as 2 in Fig. 2.4). For this reason, even though the salt concentration is high in the left side, salt molecules are carried out of the domain by the reversed flow.

3.1. Comparison of slip and no slip boundary condition

In order to clarify that the flow and mas transportation can be enhanced by the Marangoni effect, here the comparison is needed in case with Marangoni effect (namely slip boundary condition on boundary 4) and pure diffusion (namely no slip boundary condition on boundary 4). In detail, the first thing is to compare the concentration distribution in several cases of the domain in both situations. Here takes left boundary concentration $c_1 = 700 mol\, m^{-3}$ namely the concentration gradient $\Delta c = c_1 - c_0 = 100\, mol\, m^{-3}$ and the thickness of the evaporator $\delta_1 = 0.5mm$ as an example to plot the transient concentration (see fig. 3.1a). Here the concentration distribution results after 5 seconds, 5 minutes and at stationary condition are shown in both Marangoni effect (left side) and purely diffusion (right side) condition. From this plot, it is very clear that the mass transport in Marangoni effect is faster than purely diffusion. However, only with this plot is not able to explore to what extent the mass transport process is enhanced by the Marangoni effect induced flow. Thus, the ratio of molar flux out of the right boundary of the domain at the stationary state (see Fig. 3.1b) in both situations is necessary to normalize the outcome:

$$\frac{N_{slip}}{N_{no\ slip}} = \frac{\int_0^{\delta_1}(-D_i\nabla c_i + \mathbf{u}c_i)_{slip}\cdot\mathbf{n}dy}{\int_0^{\delta_1}(-D_i\nabla c_i)_{no\ slip}\cdot\mathbf{n}dy} \tag{8}$$

Where N_{slip} and $N_{no\ slip}$ is the outgoing molar fluxes (see Fig. 3.1b) in Marangoni effect and purely diffusion condition, respectively.

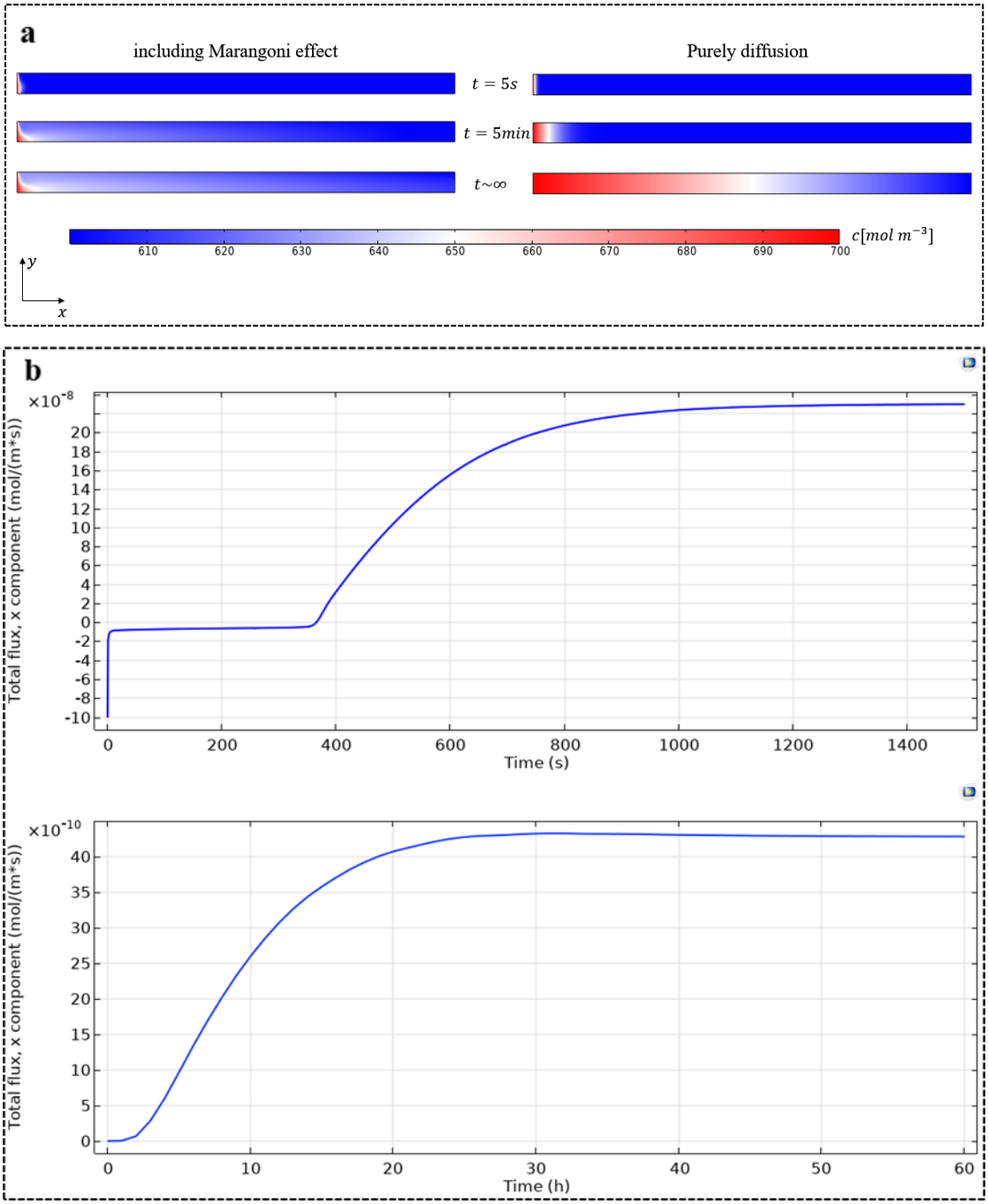

Fig. 3.1 Comparison of slip and no slip boundary condition. (a) transient concentration distribution of the domain. Left side: concentration distribution with Marangoni effect. Right side: concentration distribution with only purely diffusion. (b) Total molar flux in terms of Marangoni effect (upper one) and purely diffusion (lower one) in the condition of $\Delta c = 100\ mol\ m^{-3}$ and $\delta_1 = 0.5mm$.

According to the molar flux plots in Fig. 3.1, it is clear that the molar flux with Marangoni effect reaching to the stationary state much earlier than purely diffusion condition, which means a faster mass transport with Marangoni effect.

In this condition:

$N_{no\ slip} = 4.288 \times 10^{-9} mol/s$

$N_{slip} = 2.299 \times 10^{-7} mol/s$

Thus, the ration of molar flux in stationary condition in both cases: $\frac{N_{slip}}{N_{no\ slip}} = 53.615$.

Since the concentration gradient is related to the concentration gradient, and in order to figure out the relationship of the salt rejection performance with the thickness of the evaporator domain, the same simulation is also conducted at the condition of left boundary concentration $c_1 = 700mol\ m^{-3}$, $1000mol\ m^{-3}$, $3000mol\ m^{-3}$ and thickness $\delta_1 = 0.5mm, 1mm, 3mm, 5mm$, the result is shown in Table 3.1.

concentration c_1 / $N_{slip}/N_{no\ slip}$ / thickness	$700mol\ m^{-3}$	$1000mol\ m^{-3}$	$3000mol\ m^{-3}$
0.5mm	54.145	98.093	153.072
1mm	40.875	62.554	87.578
3mm	29.356	38.508	46.626
5mm	23.581	29.973	37.985

Table 3.1 The ratio of the molar flux flowing out of the right boundary in no slip boundary condition (purely diffusion) and slip boundary condition (including Marangoni effect) in several cases.

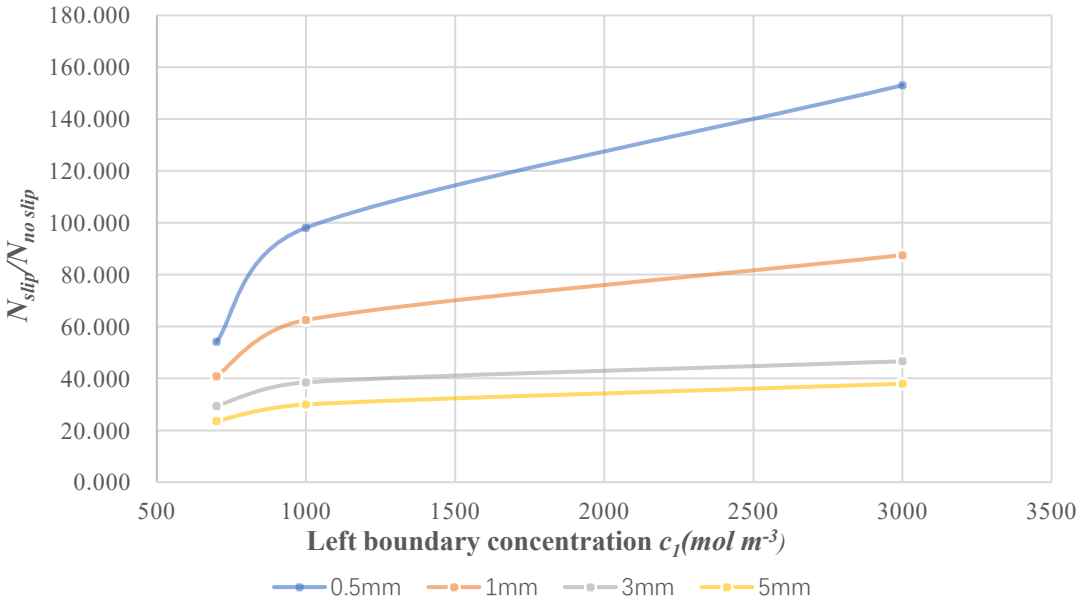

Fig. 3.2 the trend of the ratio of the molar flux flowing out of the right boundary in slip boundary condition and no slip boundary (purely diffusion) condition

It can be easily derived from the outcome of the numerical simulation that the molar flux flowing out of the domain in Marangoni effect is more than purely diffusion condition (more than 20 times according to the concentration gradient and the thickness of the evaporator), which means the concentration gradient induced Marangoni effect is quite helpful for the salt rejection of the device.

3.2. Comparison of concentration gradient

Obviously, the concentration gradient between two ends of the domain plays an important role in the Marangoni effect. From the Table 3.1 and Fig. 3.2 it can derived that with the same thickness of the evaporator, the ratio of the outgoing molar flux of Marangoni effect and purely diffusion is increasing with the rise of the concentration gradient. In order to figure out how this happened during the whole process, more figures are needed (see Fig. 3.3).

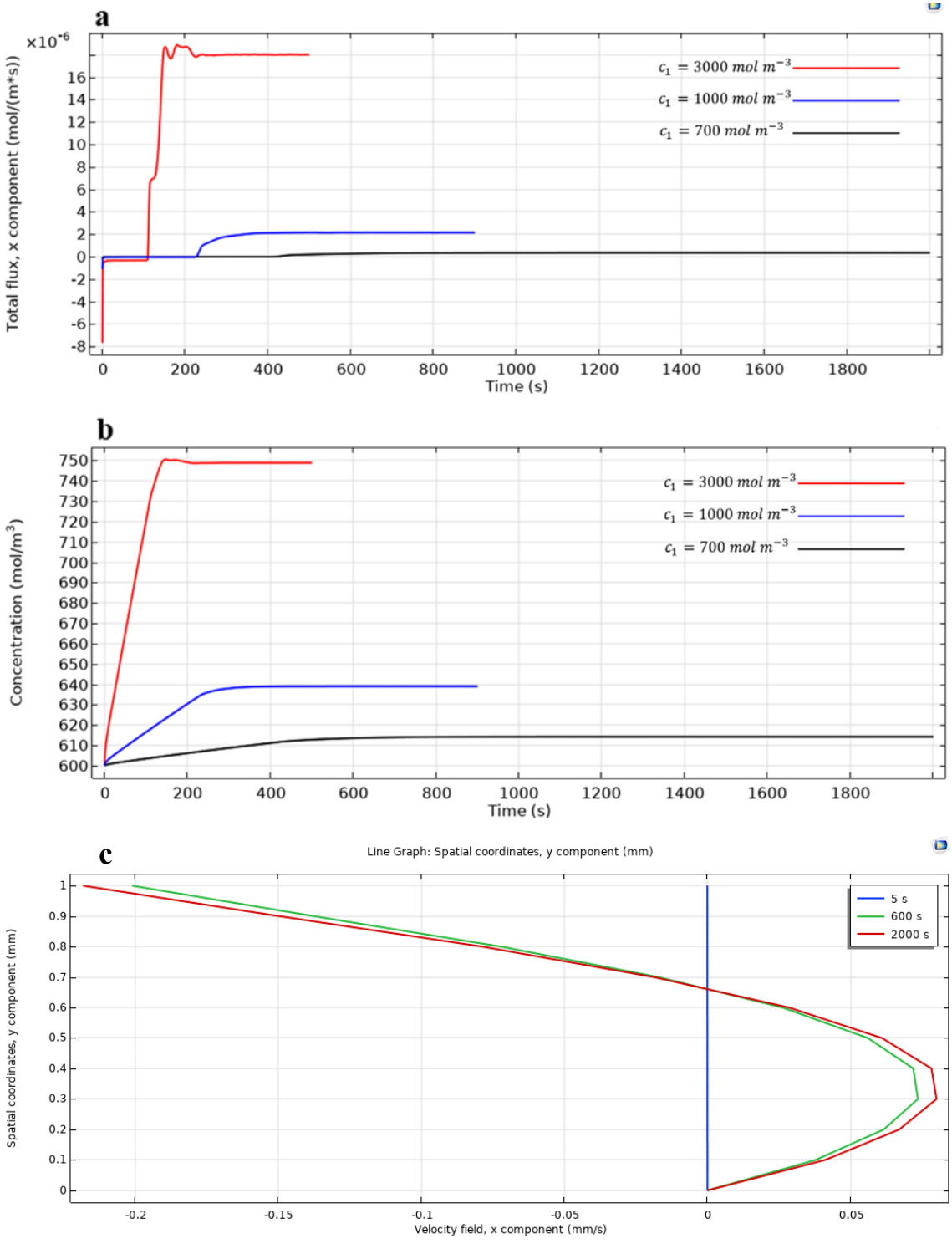

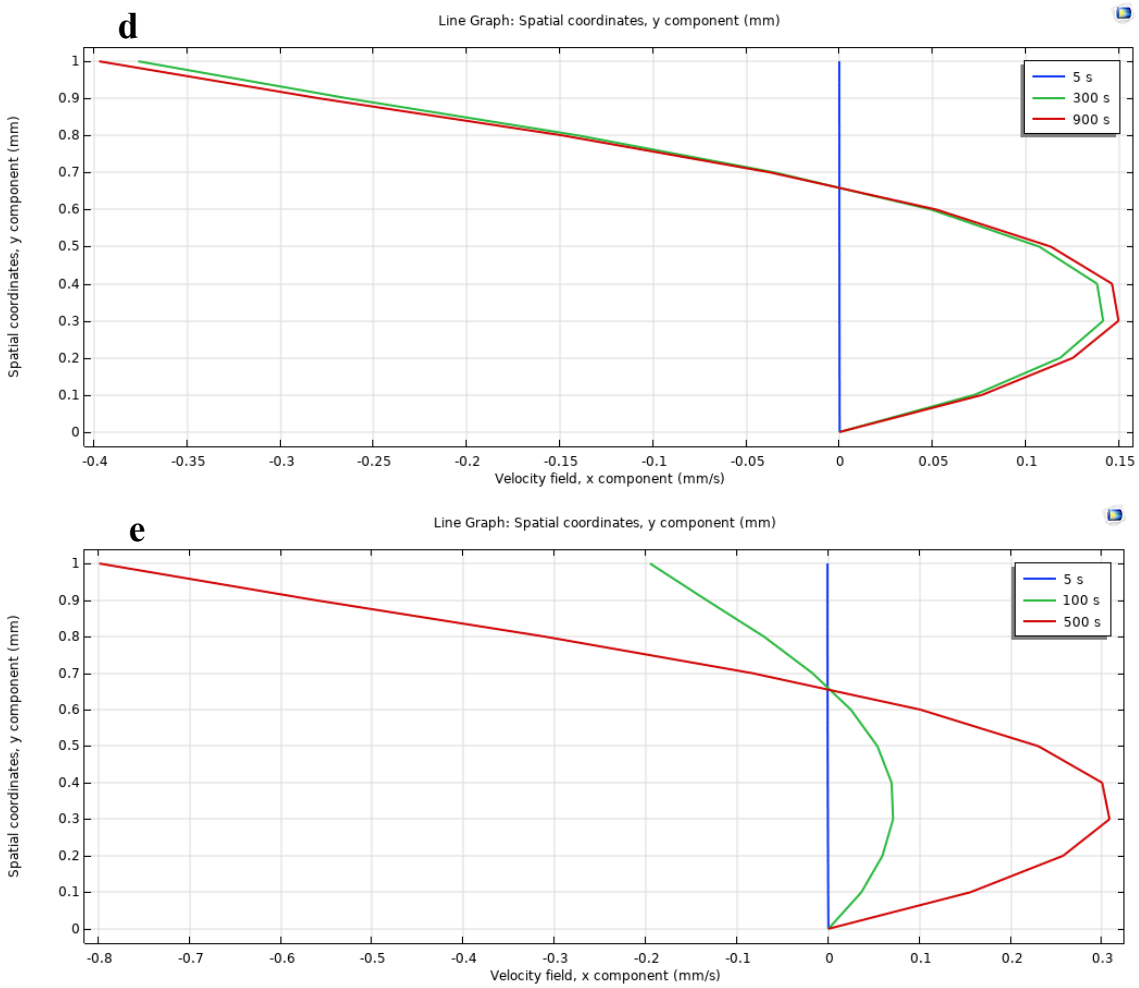

Fig. 3.3 Process of the Marangoni effect in terms of 1mm thickness with different concentration gradient. (a) the change of outgoing molar flux. (b) the change of the average surface concentration. (c) stationary velocity at $x = L$ in case of $\delta_1 = 1mm$ and $c_1 = 700\ mol\ m^{-3}$ at start, non-stationary and stationary condition. (d) stationary velocity at $x = L$ in case of $\delta_1 = 1mm$ and $c_1 = 1000\ mol\ m^{-3}$ at start, non-stationary and stationary condition. (e) stationary velocity at $x = L$ in case of $\delta_1 = 1mm$ and $c_1 = 3000\ mol\ m^{-3}$ at start, non-stationary and stationary condition.

Here, take thickness $\delta_1 = 1mm$ as example to plot the outgoing flux and average concentration at the condition of different concentration gradient. From Fig. 3.3a, not only the amount of outgoing flux is larger but also it's faster to get to the stationary condition with larger concentration, which can also be derived from the average surface concentration plot (Fig. 3.3b). The reason behind this is that with a higher salt concentration on the left boundary, there will be a larger driving force caused by Marangoni effect along the domain near the air-water interface, thus the faster reverse flow (see Fig. 3.3c, d and e), which means a better performance of salt rejection.

3.3. Comparison of different thicknesses

In order to explore the Marangoni effect in case of different thicknesses and to get the suitable thickness for the device, Here are the simulation results in terms of $c_1 = 700\ mol\ m^{-3}$.

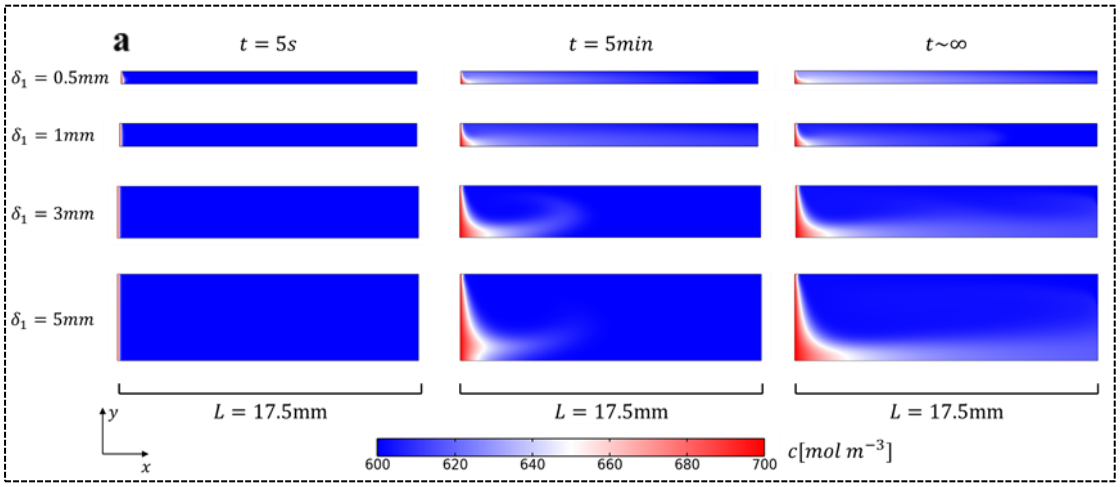
a
$t = 5s$
$t = 5min$
$t \sim \infty$
$\delta_1 = 0.5mm$
$\delta_1 = 1mm$
$\delta_1 = 3mm$
$\delta_1 = 5mm$
$L = 17.5$mm
$L = 17.5$mm
$L = 17.5$mm
y
x
600
620
640
660
680
700
$c[mol\ m^{-3}]$

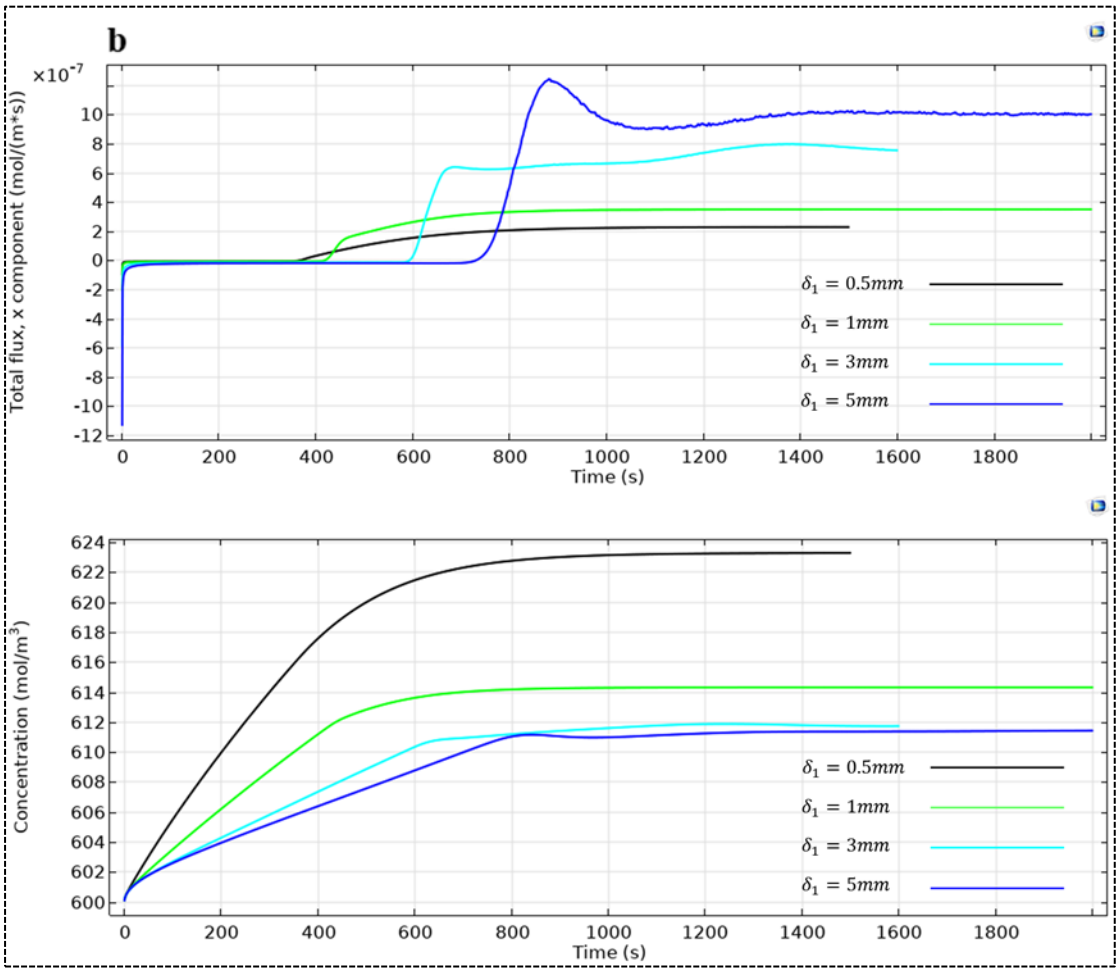
b
$\times 10^{-7}$
Total flux, x component (mol/(m*s))
10
8
6
4
2
0
-2
-4
-6
-8
-10
-12
0
200
400
600
800
1000
1200
1400
1600
1800
Time (s)
$\delta_1 = 0.5mm$
$\delta_1 = 1mm$
$\delta_1 = 3mm$
$\delta_1 = 5mm$
Concentration (mol/m^3)
624
622
620
618
616
614
612
610
608
606
604
602
600
0
200
400
600
800
1000
1200
1400
1600
1800
Time (s)
$\delta_1 = 0.5mm$
$\delta_1 = 1mm$
$\delta_1 = 3mm$
$\delta_1 = 5mm$

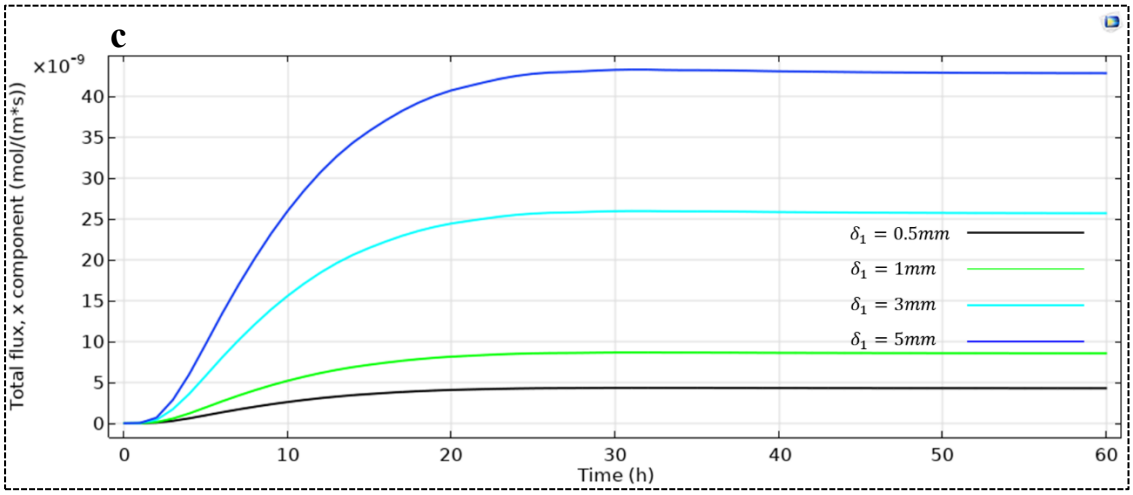

Fig. 3.4 Simulation results of different thicknesses. (a) transient surface concentration of different thicknesses under the condition of $c_1 = 700\ mol\ m^{-3}$. (b) Including Marangoni effect condition: Upper one: outgoing molar fluxes of four thicknesses. Lower one: the change of average surface concentration of four thicknesses. (c) molar flux comparison of four thicknesses under purely diffusion condition

According to the transient surface concentration plot (Fig. 3.4a), the flow moves faster alone the x direction in the case of thinner evaporator, and this can be also proved by the Fig. 3.5, which means the time used to reach the stationary state is less. However, the amount of outgoing molar flux is much smaller than thicker cases (see Fig.3.4b), since the area of the domain and the open boundary is larger for diffusion and molar flux going out. From another side, the average surface concentration at stationary state is higher in thinner cases. Besides, from Fig. 3.2, the relative ratio $N_{slip}/N_{no\ slip}$ is larger when the thickness of the domain is thinner whatever the concentration gradient is, which means that the Marangoni effect is more obvious with respect to the purely diffusion in case of thinner layer of the evaporator.

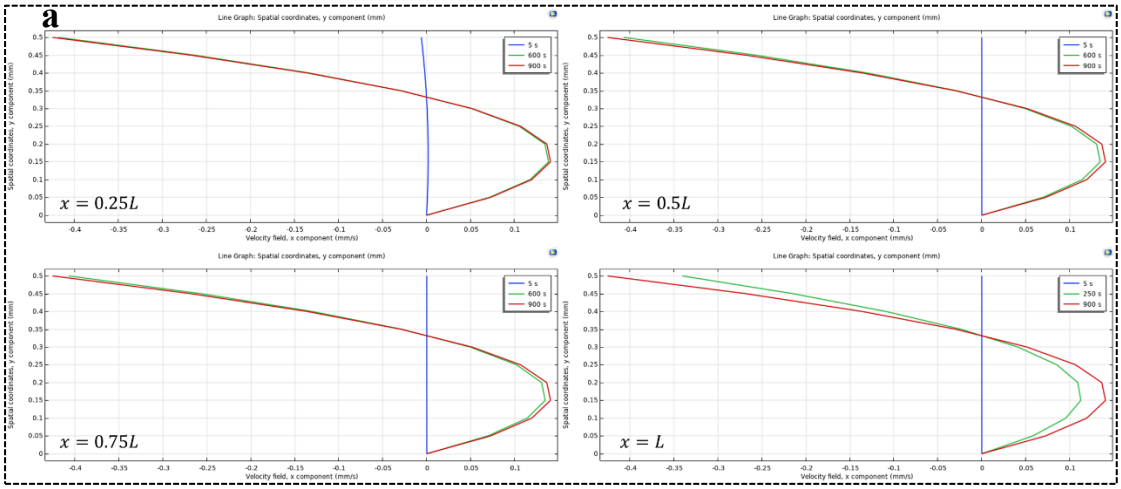

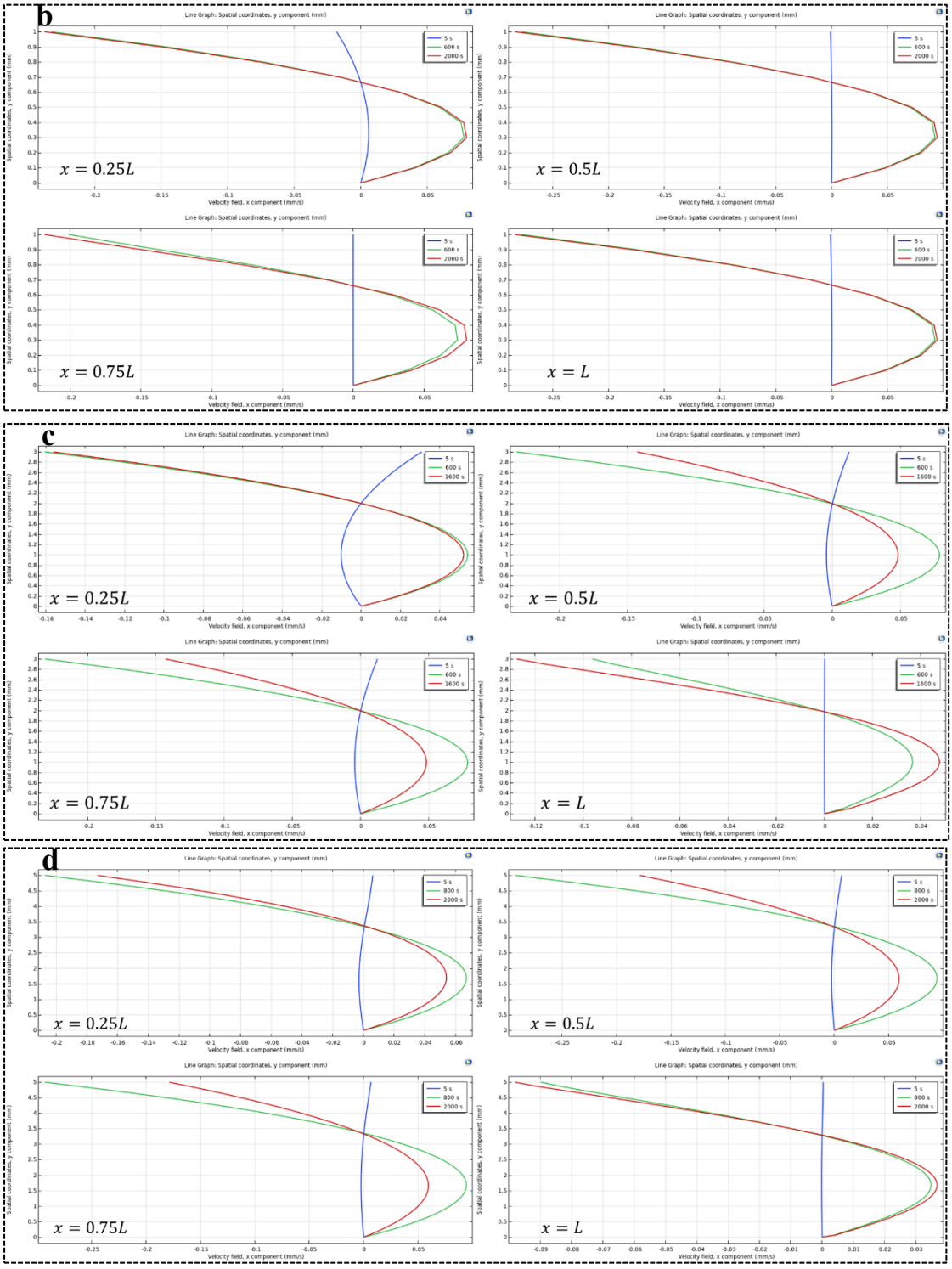

Fig. 3.5 stationary velocity at different position of the domain ($x = 0.25L, x = 0.5L, x = 0.75L$ and $x = L$ from left to right and from top to bottom) in case of $\delta_1 = 0.5mm\ (a), 1mm\ (b), 3mm\ (c) and\ 5mm\ (d)$ and $c_1 = 700\ mol\ m^{-3}$ at the time of start, non-stationary and stationary state respectively.

According to Fig. 3.5, first of all, the stationary of all cases is quite small (not consider perturbations) since the concentration at these positions does change significantly. Moreover, the stationary velocity gets to the stationary state in a faster way near the left boundary, which is caused by the fast rise of concentration in these areas. However, this phenomenon is weakened in case of thicker (3mm and 5mm) domain. The reason is

that the rate of surface concentration change is slower in these cases, which is also shown in Fig. 3.4b(lower one). Finally, because the average concentration is higher in thinner cases with the same left boundary concentration, which means more effective Marangoni effect driven flow, the stationary velocity of thicker layers in all positions is lower than thinner ones.

4. Conclusions and perspectives

Since the desalination device is invented, the salt accumulation remains a big challenge, especially for solar passive distiller. Although there have been many types of new materials and structures being discussed to solve this problem, the application of those technologies is complicated. In this study several cases of desalination device are introduced in terms of advantages and disadvantages. Also, a new type of solar passive distiller proposed by professor Morciano and coworker is introduced. Unlike anti-clogging solar passive distillers discussed in previous passages which rely on new types of materials and configurations (which means more cost and harder for maintenance), this device provides the primary reason of the salt rejection. In their work, for the first time, the Marangoni effect is related to the salt rejection phenomenon, and the whole configuration and some other components are optimized to improve the efficiency and the salt rejection performance of the device.

4.1. Conclusions

Based on their study, this passage mainly focuses on the boundary condition and the configuration of the horizontal evaporator layer. In detail, the 2-D model of the evaporator is built in COMSOL Multiphysics and the relationship of the concentration gradient between two ends of the domain and the Marangoni effect is studied with different left boundary concentration through numerical simulation. Besides, by analyzing the data and results of the simulation in case of several thicknesses of the domain, such conclusion can be derived:

1) Higher concentration gradient means more effective Marangoni effect.
2) Evaporator with thinner thickness has more obvious Marangoni effect with respect to the purely diffusion.
3) More outgoing fluxes is shown in case of thicker Evaporator

However, these conclusions are made without thinking the whole device, although the thinner evaporator has a better performance in terms of Marangoni effect, the heat energy transported to the evaporator and the evaporation rate must be considered, when the evaporator is thin, the amount of salt water stored in this layer is not too much, in this condition, if the process of evaporation is faster than the salt rejection process which related to the Marangoni effect driven flow, there will be salt accumulation and thus clogging. Besides, based on the study of concentration gradient, the initial value of the salt concentration at the middle part of the evaporator (left boundary of the domain) should be considered a point to further improve the salt rejection performance. Furthermore, the wick ability of the material should be also related to the whole process, the purpose is to control the salt water supply to the horizontal evaporator so that to keep a balance between the evaporation rate and the salt rejection rate in the condition of best salt rejection performance during most time of the day. Consequently, it would be possible to reach a higher productivity of fresh water and further decrease the cost for getting drinkable water, thus making solar passive distiller a more cheap, green and general technology in the future.

4.2. Perspectives

This study is mainly focused on how to improve the Marangoni effect to get a higher salt rejection rate for solar passive distiller by changing the evaporator layer, based on this study, more research has to be conducted towards optimized hydrophilic materials with anti-fouling properties and tailored capillary action so that a solar passive distiller with more stages and larger size can be fed with salt water and the Marangoni-driven flow can be optimized. In this way, it would be possible to further increase the productivity and to lower the cost of the desalinated water, thus increasing the competitiveness of the solar passive desalination device with respect to active technologies.

[1] S. Ahuja, "Overview of Global Water Challenges and Solutions," *Water Challenges and Solutions on a Global Scale*, ACS Symposium Series, pp. 1-25, 2015.

[2] S. W. Sharshir, G. Peng, A. H. Elsheikh, E. M. A. Edreis, M. A. Eltawil, T. Abdelhamid, A. E. Kabeel, J. Zang, and N. Yang, "Energy and exergy analysis of solar stills with micro/nano particles: A comparative study," *Energy Conversion and Management,* vol. 177, pp. 363-375, 2018.

[3] C. P. Kelley, S. Mohtadi, M. A. Cane, R. Seager, and Y. J. P. o. t. n. A. o. S. Kushnir, "Climate change in the Fertile Crescent and implications of the recent Syrian drought," vol. 112, no. 11, pp. 3241-3246, 2015.

[4] M. M. Mekonnen, and A. Y. J. S. a. Hoekstra, "Four billion people facing severe water scarcity," vol. 2, no. 2, pp. e1500323, 2016.

[5] E. Chiavazzo, M. Morciano, F. Viglino, M. Fasano, and P. Asinari, "Passive solar high-yield seawater desalination by modular and low-cost distillation," *Nature Sustainability,* vol. 1, no. 12, pp. 763-772, 2018.

[6] G. Micale, L. Rizzuti, and A. Cipollina, *Seawater Desalination: Conventional and Renewable Energy Processes*, **2009**.

[7] L. Sahota, and G. N. Tiwari, "Effect of nanofluids on the performance of passive double slope solar still: A comparative study using characteristic curve," *Desalination,* vol. 388, pp. 9-21, 2016.

[8] V. Velmurugan, M. Gopalakrishnan, R. Raghu, and K. Srithar, "Single basin solar still with fin for enhancing productivity," *Energy Conversion and Management,* vol. 49, no. 10, pp. 2602-2608, 2008.

[9] A. E. Kabeel, "Performance of solar still with a concave wick evaporation surface," *Energy,* vol. 34, no. 10, pp. 1504-1509, 2009.

[10] M. Zerrouki, N. Settou, Y. Marif, and M. M. Belhadj, "Simulation study of a capillary film solar still coupled with a conventional solar still in south Algeria," *Energy Conversion and Management,* vol. 85, pp. 112-119, 2014.

[11] K. K. Matrawy, A. S. Alosaimy, and A. F. Mahrous, "Modeling and experimental study of a corrugated wick type solar still: Comparative study with a simple basin type," *Energy Conversion and Management,* vol. 105, pp. 1261-1268, 2015.

[12] V. Kashyap, A. Al-Bayati, S. M. Sajadi, P. Irajizad, S. H. Wang, and H. Ghasemi, "A flexible anti-clogging graphite film for scalable solar desalination by heat localization," *Journal of Materials Chemistry A,* vol. 5, no. 29, pp. 15227-15234, 2017.

[13] P. Pal, P. Yadav, R. Dev, and D. Singh, "Performance analysis of modified basin type double slope multi–wick solar still," *Desalination,* vol. 422, pp. 68-82, 2017.

[14] G. Ni, S. H. Zandavi, S. M. Javid, S. V. Boriskina, T. A. Cooper, and G. Chen, "A salt-rejecting floating solar still for low-cost desalination," *Energy & Environmental Science,* vol. 11, no. 6, pp. 1510-1519, 2018.

[15] S. He, C. Chen, Y. Kuang, R. Mi, Y. Liu, Y. Pei, W. Kong, W. Gan, H. Xie, E. Hitz, C. Jia, X. Chen, A. Gong, J. Liao, J. Li, Z. J. Ren, B. Yang, S. Das, and L.

Hu, “Nature-inspired salt resistant bimodal porous solar evaporator for efficient and stable water desalination,” *Energy & Environmental Science,* vol. 12, no. 5, pp. 1558-1567, 2019.

[16] Y. Xia, Q. Hou, H. Jubaer, Y. Li, Y. Kang, S. Yuan, H. Liu, M. W. Woo, L. Zhang, L. Gao, H. Wang, and X. Zhang, “Spatially isolating salt crystallisation from water evaporation for continuous solar steam generation and salt harvesting,” *Energy & Environmental Science,* vol. 12, no. 6, pp. 1840-1847, 2019.

[17] A. Saravanan, and M. Murugan, “Performance evaluation of square pyramid solar still with various vertical wick materials – An experimental approach,” *Thermal Science and Engineering Progress,* vol. 19, 2020.

[18] J. Xu, Z. Wang, C. Chang, B. Fu, P. Tao, C. Song, W. Shang, and T. Deng, “Solar-driven interfacial desalination for simultaneous freshwater and salt generation,” *Desalination,* vol. 484, 2020.

[19] Z. Xu, L. Zhang, L. Zhao, B. Li, B. Bhatia, C. Wang, K. L. Wilke, Y. Song, O. Labban, J. H. Lienhard, R. Wang, and E. N. Wang, “Ultrahigh-efficiency desalination via a thermally-localized multistage solar still,” *Energy & Environmental Science,* vol. 13, no. 3, pp. 830-839, 2020.

[20] Y. Shi, C. Zhang, R. Li, S. Zhuo, Y. Jin, L. Shi, S. Hong, J. Chang, C. Ong, and P. Wang, “Solar Evaporator with Controlled Salt Precipitation for Zero Liquid Discharge Desalination,” *Environ Sci Technol,* vol. 52, no. 20, pp. 11822-11830, Oct 16, 2018.

[21] E. Strobach, B. Bhatia, S. Yang, L. Zhao, and E. N. J. J. o. N.-C. S. Wang, “High temperature annealing for structural optimization of silica aerogels in solar thermal applications,” vol. 462, pp. 72-77, 2017.

[22] L. A. Weinstein, K. McEnaney, E. Strobach, S. Yang, B. Bhatia, L. Zhao, Y. Huang, J. Loomis, F. Cao, and S. V. J. J. Boriskina, “A hybrid electric and thermal solar receiver,” vol. 2, no. 5, pp. 962-975, 2018.

[23] L. Zhao, B. Bhatia, S. Yang, E. Strobach, L. A. Weinstein, T. A. Cooper, G. Chen, and E. N. J. A. n. Wang, “Harnessing heat beyond 200° C from unconcentrated sunlight with nonevacuated transparent aerogels,” vol. 13, no. 7, pp. 7508-7516, 2019.

[24] M. Morciano, M. Fasano, S. V. Boriskina, E. Chiavazzo, and P. Asinari, “Solar passive distiller with high productivity and Marangoni effect-driven salt rejection,” *Energy & Environmental Science,* vol. 13, no. 10, pp. 3646-3655, 2020.

[25] M. G. Velarde, and R. K. Zeytounian, *Interfacial phenomena and the Marangoni effect*: Springer, 2002.

[26] H. Kitahata, and N. J. T. J. o. c. p. Yoshinaga, “Effective diffusion coefficient including the Marangoni effect,” vol. 148, no. 13, pp. 134906, 2018.

[27] K. Mills, B. Keene, R. Brooks, A. J. P. T. o. t. R. S. o. L. S. A. M. Shirali, Physical, and E. Sciences, “Marangoni effects in welding,” vol. 356, no. 1739, pp. 911-925, 1998.

[28] P. Lee, P. Quested, M. J. P. T. o. t. R. S. o. L. S. A. M. McLean, Physical, and E. Sciences, “Modelling of Marangoni effects in electron beam melting,” vol. 356,

no. 1739, pp. 1027-1043, 1998.
[29] H. C. Kuhlmann, *Thermocapillary convection in models of crystal growth*, 1999.
[30] H. Hu, and R. G. J. T. J. o. P. C. B. Larson, "Marangoni effect reverses coffee-ring depositions," vol. 110, no. 14, pp. 7090-7094, 2006.
[31] F. Toldrá, *Dry-cured meat products*: John Wiley & Sons, 2008.
[32] K. Nayar, D. Panchanathan, G. McKinley, J. J. J. o. P. Lienhard, and C. R. Data, "Surface tension of seawater," vol. 43, no. 4, pp. 043103, 2014.
[33] M. H. Sharqawy, J. H. Lienhard, S. M. J. D. Zubair, and w. Treatment, "Thermophysical properties of seawater: a review of existing correlations and data," vol. 16, no. 1-3, pp. 354-380, 2010.